Finite Element Analysis of Structures

Comparing Large and Small-Scale Structures in Linear and Non-linear Behaviour

CTB3000-16: Bachelor Thesis

Amine Alami

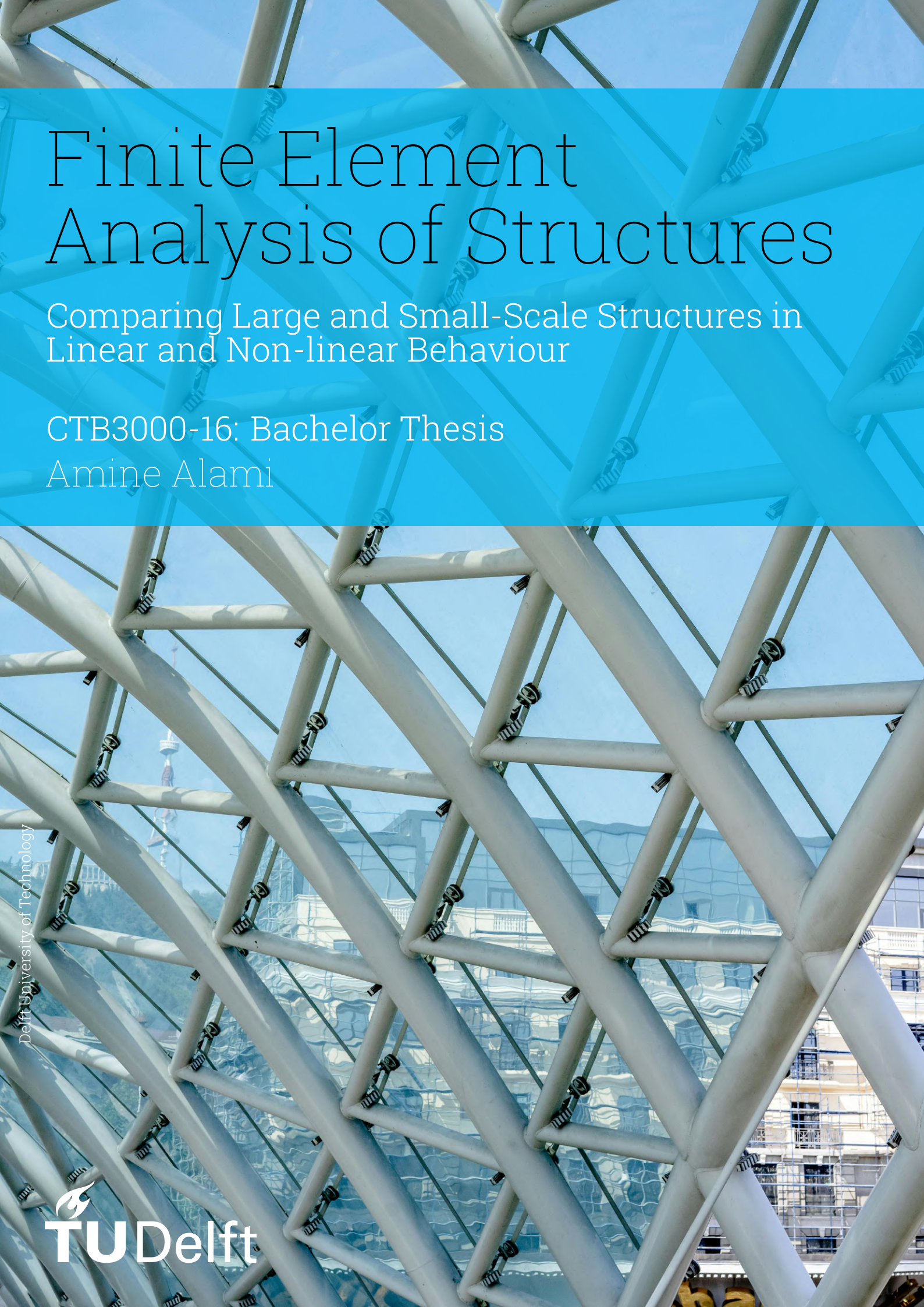

Delft University of Technology

TU Delft

Finite Element Analysis of Structures

Comparing Large and Small-Scale Structures in Linear and Non-linear Behaviour

by

Amine Alami

to obtain the degree of Bachelor of Science
at Delft University of Technology,
to be defended publicly on Tuesday June 25, 2024 at 10:00 AM.

Student number:	5446392	
Project duration:	April 22, 2024 – June 24, 2024	
Thesis committee:	Dr. ir. P. C. J. Hoogenboom	TU Delft, supervisor 1
	Ir. T. Gärtner	TU Delft, supervisor 2

Cover: P, O. (2021, September 1). Metal frames of a dome building · free stock photo. https://www.pexels. com/photo/metal-frames-of-a-dome-building-9397568/ 7

TU Delft

Preface

This bachelor thesis represents a significant milestone in my academic journey at the Delft University of Technology. The research and analysis presented herein are focused on a specialized area within civil engineering, requiring a solid foundation in applied mechanics for thorough comprehension.

I would like to express my gratitude to Dr. Ir. P.C.J. Hoogenboom and Ir. T. Gärtner for their support throughout this project.

To the readers, I hope this thesis provides valuable insights and contributes meaningfully to the field of civil engineering. Your understanding and appreciation of the work will be greatly enhanced with a background in applied mechanics. Thank you for your interest and engagement with this research.

Amine Alami
Delft, June 2024

Summary

The use of computers in engineering started in 1960. Before 1960, engineers used physical models to check the results of complex structures. Recently, these physical models have been used for education purposes, namely, in the minor *Bend and Break*. Conversion from small-scale structures to real-sized structures was taught in this minor (P. C. J. Hoogenboom, n.d.). Therefore, This research aims to find a relation between small-scale and real-sized structures. Namely, the conversion of internal forces and displacements from a small-scale structure to a real-sized structure in both linear and non-linear material behaviour. A linear calculation yields a linear relation between the results and the applied force on the structure, unlike a non-linear calculation. The conversion rules apply to linear material behaviour. However, whether they also apply to physical and geometrical non-linear material behaviour is uncertain. This uncertainty yields the following research question:

"There are conversion rules for deflection and stresses from small-scale structures to real-sized structures. Do these apply to non-linear behaviour too?"

Multiple structures were analysed. A small-scale and real-sized model of these structures was modelled in the finite element program SCIA Engineer (SCIA, 2024). The geometrical properties of the small-scale structures were 10 times smaller than the geometrical properties of the real-sized structures. The type of structures is itemized below:

- A steel truss (with and without bending stiffness)
- A steel beam (statically determinate and statically indeterminate)
- A steel Vierendeel girder
- A concrete two-way slab
- A concrete shell roof

Geometrical and physical non-linear calculations were done. The geometrical non-linearity focused on local and global buckling, which yields large displacements while physical non-linearity focused on the plasticity of hinges and elastoplastic stress-strain diagrams. Relevant forces in the structures' members and nodes were computed with linear and non-linear calculations. Additionally, displacement and deformations of relevant members or nodes were analysed. Furthermore, the applied loads are point loads, line loads or distributed loads, which had their conversion rules from small-scale to real-sized structures. Namely, the real-sized point load is 100 times larger than the small-scale point load. The real-sized line load is 10 times larger than the small-scale line load and distributed loads are identical in both structures. This yields identical stresses in the small-scale and real-sized structures. Displacements differ by a factor of 10 and internal forces by a factor of 100 or 1000, depending on the type of applied load.

The steel trusses, the statically determinate beam, the Vierendeel girder and the concrete shell roof were all analysed with a geometrical non-linear calculation. All linear analyses followed the conversion rules perfectly. The relevant displacements in the small-scale structures differed by a factor of 10 from the displacements in the real-sized structures. The internal forces differed by a factor of 100 or 1000. Similarly, in the geometrical non-linear calculation, the displacements differed by a factor of 10 and the internal forces by a factor of 100 or 1000. However, there were small numerical errors in the non-linear calculation. This happens when SCIA Engineer makes a non-linear calculation due to its iterative calculation method. The statically indeterminate beam and the concrete two-way slab were analysed with a physical non-linear calculation in addition to geometrical non-linearity. The plasticity of hinges was tested in the statically indeterminate beam and the elastic stress-strain curve of the two-way slab model was changed to an elastoplastic stress-strain curve which yields large displacements. Again, the internal forces differed by a factor of 100 or 1000, depending on the type of applied load. The

displacements differed by a factor of 10, which is in line with the existing conversion rules.

In conclusion, for the analysed structures, the conversion rules apply to both geometrical and physical non-linear material behaviour.

Contents

List of Figures

List of Tables

Nomenclature

Abbreviations

Abbreviation	Definition
FEA	Finite Element Analysis
RS	Real-Sized
SS	Small-Scaled

Symbols

Symbol	Definition	Unit
A	Cross-sectional area	[m^2]
E	Young's Modulus	[N/mm^2]
f	Externally applied force vector on node or member	[kN]
I	Moment of inertia area	[m^4]
K	Stiffness Matrix	[kN/m]
u	Displacement vector on node or member	[mm]

1 Introduction

In Civil and Structural Engineering, we design large complex structures in which structural safety is the most important aspect. In general, a design starts with a well-elaborated plan. The position and orientation of columns and beams are planned and building materials are chosen (Mishra, 2024). In this phase, all geometrical and material properties are designed. Subsequently, the permanent and variable loads and their combinations acting on the structure are computed, followed by the internal reaction forces, stresses and displacements. An interesting way to estimate these forces and displacements is by designing a scaled version of the corresponding structure. Subsequently, the displacements are measured and the applied forces are computed. Rescaling the structure to its original dimensions yields results applicable to the real-sized structure. The applied forces and displacements in the real-sized structure can be computed by scaling these applied forces and displacements of the small-scale structures with a set of conversion rules.

It is unknown whether the conversion method works for non-linear material behaviour. Imperfections of members, materials and connections are not taken into account in a model computed with a linear calculation. Subjecting the structure to non-linear material behaviour or imperfections can change the conversion rules from scaled to real-sized structures. This uncertainty can be problematic for the use of this method because the obtained results for the real-sized structure could become inaccurate when using conversion rules for linear material properties without knowing if these conversion rules apply to non-linear material properties.

The goal of this research is to find out whether small-scale structures subjected to forces that yield non-linear material behaviour can be converted into real-sized structures with a set of conversion rules. The following research question is answered:

"***There are conversion rules for deflection and stresses from small-scale structures to real-sized structures. Do these apply to non-linear material behaviour too?***"

The research is limited to finite element models of a set of structures, focusing on steel and concrete. This selection consists of a steel truss, a concrete slab (floor), a concrete shell roof and a steel Vierendeel girder.

The structure of the report is as follows. Chapter 2 dives into the theoretical background of Finite element analysis, a powerful numerical tool to compute all relevant quantities. Furthermore, it gives an elaborate explanation of linear and non-linear material behaviour and their distinctions. The selection of structures and the general conversion rules follow in Chapter 3. In Chapters 4, 5, 8, 7 and 6 the selection of structures is tested on linear and non-linear material behaviour in the Finite element Analysis (FEA) program SCIA Engineer (SCIA, 2024). All structures, small-scale and real-sized are modelled in this software-packet. Finally, a conclusion to the research question is formed in Chapter 9.

2
Theoretical framework

As mentioned in the introduction, finite element analysis is a powerful numerical method developed to analyse the mechanical behaviour of complex engineering structures. Its concept originates from the time of Archimedes, who tried to compute areas of complex shapes by dividing them into multiple triangles. This is very similar to finite element analysis. Namely, when performing a finite element analysis on a structure, it is divided into small elements for which the forces, stresses and displacements are approximated (Sabat & Kundu, 2020).

This chapter, explains the fundamentals of finite element analysis and gives a simple example. Additionally, linear and non-linear material behaviour are explained.

2.1. Fundamentals of Finite Element Analysis

The process of finite element analysis can be subdivided into three processes. First, a structure needs to be modelled in a FEA (finite element analysis) program. The structure consists of a discrete amount of nodes and members, for which applied loads or displacements are chosen. Second, the FEA program constructs and solves a system of either linear or non-linear equations. A general expression of the constructed matrices follows Hooke's Law (Cantor, 2020) and is shown in Equation 2.1

$$\mathbf{Ku} = \mathbf{f}, \tag{2.1}$$

where $\boldsymbol{u}$ is the displacement vector and $\boldsymbol{f}$ is the applied force vector on each finite element. The $\boldsymbol{K}$ matrix usually consists of the stiffnesses of the individual elements, but it changes according to the type of the assessed structure. Finally, the obtained results are graphed or tabulated (Roylance, 2001).

A brief example of a finite element model is shown. Suppose there is a simply supported 1D beam, depicted in Figure 2.1 with an external point load F at the midspan. The degrees of freedom are rotation around the y-axis and displacement in the z-axis. The reaction forces are moments, shear forces and normal forces.

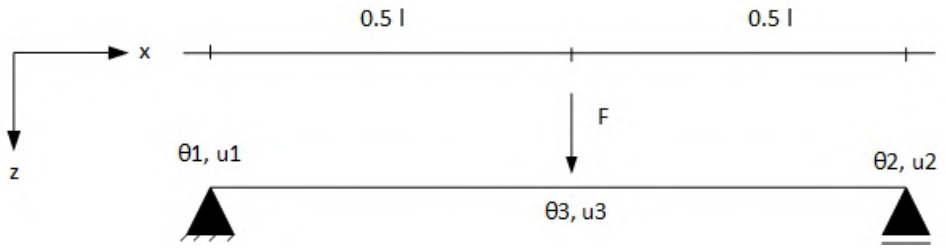

Figure 2.1: A simply supported beam subjected to a force at midspan. An example of finite element analysis is shown using this structure.

The beam has a Young's Modulus E (Çopuroğlu, 2018), a moment of inertia in the direction of loading I and a cross-sectional area A. To simplify this example, the finite element model is reduced to one member and two nodes. At the supports, the rotations around the y-axis θ_1 (left support) and θ_2 (right support) are non-zero. θ_3 at the midspan is zero due to the symmetry of loading. Furthermore, the

displacement of both supports is zero and the displacement is maximum at midspan. Thus, there are four unknown parameters in the element stiffness matrices $\boldsymbol{K_1}$ and $\boldsymbol{K_2}$ and six in the global stiffness matrix $\boldsymbol{K_{global}}$. This example only shows the final expressions of both element stiffness matrices and the global stiffness matrix. `The element stiffness matrices`[1] and displacement/rotation vector for elements 1 and 2 are shown in Equation 2.2 and Equation 2.3 depicts the global stiffness matrix and the global displacement vector.

$$\mathbf{K}_1\mathbf{u}_1 = \frac{8EI}{l^3}\begin{bmatrix} 12 & 3l & -12 & 3l \\ 3l & l^2 & -3 & \frac{1}{2}l^2 \\ -12 & -3l & 12 & -3l \\ 3l & \frac{1}{2}l^2 & -3l & l^2 \end{bmatrix}\begin{bmatrix} u_1 \\ \theta_1 \\ u_2 \\ \theta_2 \end{bmatrix}, \quad \mathbf{K}_2\mathbf{u}_2 = \frac{8EI}{l^3}\begin{bmatrix} 12 & 3l & -12 & 3l \\ 3l & l^2 & -3 & \frac{1}{2}l^2 \\ -12 & -3l & 12 & -3l \\ 3l & \frac{1}{2}l^2 & -3l & l^2 \end{bmatrix}\begin{bmatrix} u_2 \\ \theta_2 \\ u_3 \\ \theta_3 \end{bmatrix} \tag{2.2}$$

$$\mathbf{K}_{\text{global}}\mathbf{u}_{\text{global}} = \frac{8EI}{l^3}\begin{bmatrix} 12 & 3l & -12 & 3l & 0 & 0 \\ 3l & l^2 & -3l & \frac{1}{2}l^2 & 0 & 0 \\ -12 & -3l & 24 & 0 & -12 & 3l \\ 3l & \frac{1}{2}l^2 0 & 2l^2 & -3l & \frac{1}{2}l^2 & \\ 0 & 0 & -12 & -3l & 12 & -3l \\ 0 & 0 & 3l & \frac{1}{2}l^2 & -3l & l^2 \end{bmatrix}\begin{bmatrix} u_1 \\ \theta_1 \\ u_2 \\ \theta_2 \\ u_3 \\ \theta_3 \end{bmatrix} \tag{2.3}$$

The global stiffness matrix already becomes large when the structure is divided into two elements. This model is limited to computing displacements and rotations only at the supports and the midspan, whereas a finite element model on a computer provides results at numerous locations throughout the beam. The computer divides the beam into more elements, which means that the global stiffness matrix is much larger. Namely, a simply supported beam divided into 10 elements yields a global stiffness matrix of 22 by 22 instead of the 6 by 6 matrix in this example.

2.2. Linear and non-linear material behaviour

This section explains two types of material behaviour, namely, linear and non-linear material behaviour.

2.2.1. Linear material behaviour

Linear analysis is defined as any analysis where linear extrapolation of stress, load and deflection is valid (Chan, 2001). This statement holds for the linear part of a $\sigma - \epsilon$ diagram. A $\sigma - \epsilon$ diagram for construction steel is shown in Figure 2.2.

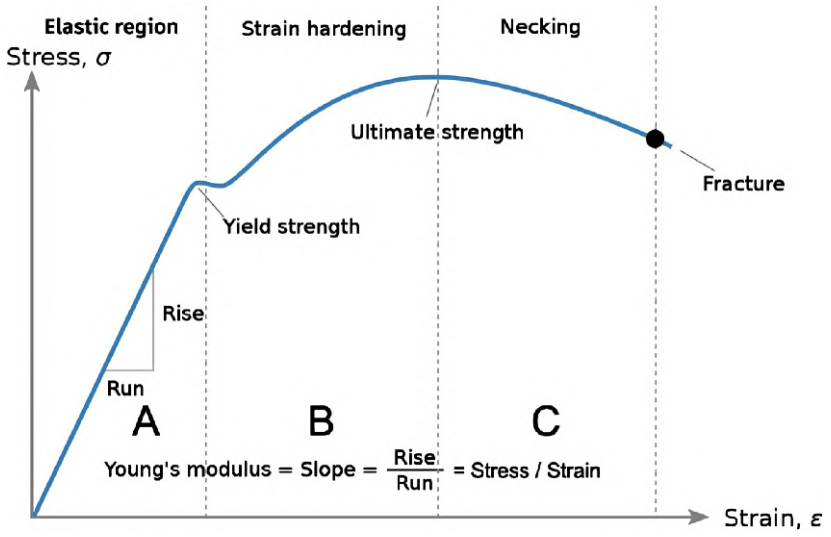

Figure 2.2: $\sigma - \epsilon$ diagram for construction steel, (Alsayed, 2021).

[1]The element stiffness matrices were made by following a finite element method lecture on YouTube. The link to the video is: https://www.youtube.com/watch?v=KWmsolAmEn4&ab_channel=MechanicalEngineeringE-Learning

This linear part can be described by Hooke's Law (Cantor, 2020). The tangent of the stress-strain relation is the Young's modulus (Çopuroğlu, 2018). It is constant in this linear part. However, for stress values higher than the yield strength, it reaches its ultimate strength and subsequently the material fractures.

The stress-strain diagram illustrated in Figure 2.2 is obtained by applying an increasing tensile force on a steel bar. Then, its elongation is measured and converted to strain. The forces are converted to stresses. The stresses and strains can be computed as described in Equations 2.4 and 2.5

$$\sigma = \frac{F}{A_0}, \tag{2.4}$$

$$\epsilon = \frac{\Delta l}{l_0}, \tag{2.5}$$

where F is the increasing tensile force, A_0 is the initial cross-sectional area of the rod, Δl is its elongation and l_0 is its initial length (Davis, 2004). When performing a compression test on a steel rod, the buckling resistance is eventually reached. Figure 2.3 shows a force-displacement diagram for a compressive test.

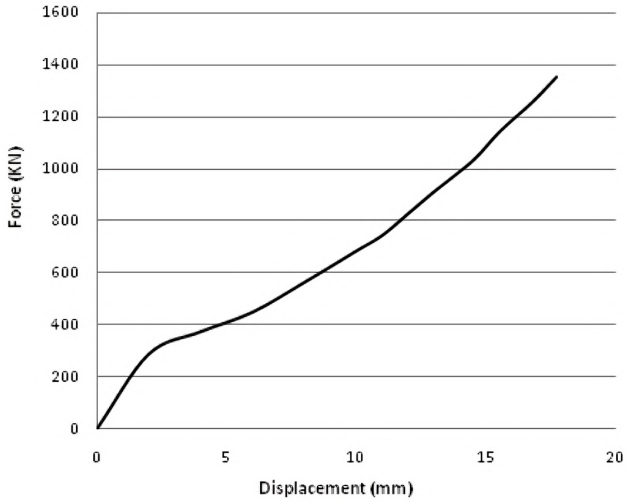

Figure 2.3: Force-Displacement diagram of a compression test on a steel member, (Ahmadpour et al., 2017).

This diagram starts as a linear relation between the applied compressive force and displacement. The relation changes for values close to the buckling resistance.

2.2.2. Non-linear material behaviour

"Non-linear analysis can be defined as any analysis when linear extrapolation of stress, load and deflection is invalid (Chan, 2001, p. 1218)." There are different types of non-linear material behaviour. For example, the moment steel starts to yield, the stress-strain relation becomes non-linear. This can be seen in Figure 2.2. Figure 2.3 also shows that the curve becomes non-linear as the buckling resistance is reached.

Another way to look at non-linear material behaviour is by testing the geometry of the structure. Geometrical non-linearity occurs when the displacements become large enough that they will affect the response of the structure. For example, when the point load F on the simply supported beam in Figure 2.1 becomes too large, additional horizontal tensile forces form at the supports. These horizontal forces would not occur for small displacements. These extra tensile forces and displacements are called second-order effects.

3 Methodology

This chapter gives a brief explanation of the selection of tested structures. Second, the conversion rules, that are proven for linear material behaviour, are presented.

3.1. Selection of tested structures

A selection of structures is chosen to be modelled in SCIA Engineer (SCIA, 2024). For each selection, two versions are modelled, a small-scale version and a real-sized version. The selected structures are the following:

- A steel truss.
- The critical buckling beam in the steel truss.
- A steel Vierendeel Girder.
- A concrete shell roof.
- A concrete one-way slab.

These structures are all analysed similarly. First, a calculation following linear material behaviour is done, in which the structures are subjected to a variety of loads increasing with a constant step size. Subsequently, either a geometrical non-linear calculation or a physical non-linear calculation is performed. The main objective for the geometrical non-linear calculation is the buckling of the structure. The scope of the physical non-linearity is the plasticity of hinges and large displacements due to the yielding of material.

Steel truss

Trusses are widely used in civil and structural engineering (Machacek & Cudejko, 2011). Therefore, this is the first structure that is assessed. The self-weight is neglected when computing the internal forces and displacement in the SCIA Engineer simulation because the conversion rules do not apply when this is considered. This structure is subjected to point loads on the nodes to avoid bending moments in members of the truss because, in practice, trusses are rarely loaded in the members but at intersections between members (Saliklis, 2020). Furthermore, this truss is modelled in a 2D environment (xz-plane) in SCIA Engineer. There are no rotations around the x-axis and z-axis. Displacements and rotation only take place in this xz-plane.

Critical buckling beam in the steel truss

As mentioned in Chapter 2, a buckling graph consists of a linear and non-linear part. Therefore, the critical buckling beam in the truss is modelled. It is a simply supported beam with a buckling length equal to the system's length. This beam is also modelled in the xz-planes and similar conditions for rotation and displacement apply. Self-weight is again neglected.

Steel Vierendeel Girder

A Vierendeel girder is a structure named after Jules Arthur Vierendeel (Pons-Poblet, 2019). It looks very similar to a truss. However, it does not have inclined members. This structure is subjected to point loads on all upper nodes. It is modelled in 2D and there are only rotations and displacements in the xz-plane.

Concrete two-way slab

A practical example of a concrete two-way slab is a floor. The chosen concrete strength class for the two-way is C30/37. In contrast with the shell roof, a slab is not prone to buckling as it transfers the loads by bending. Therefore, the concrete shell roof is assessed by changing the material behaviour from elastic to elastoplastic following Von-Mises' yield criterion (Kavoura et al., 2022). This results in large displacements as the material behaviour changes as the stresses become higher. The large displacements can be described as geometrical non-linear behaviour, which is the scope of this research.

Concrete shell roof

Another widely used building material is concrete. It is composed of three main ingredients. Namely, cement, aggregates and water (Neville, 2001). It can only withstand compressive forces and its tensile strength is negligible. Therefore, all concrete structures are reinforced for additional tensile capacity or prestressed for additional compressive stress. Therefore a higher tensile force is needed to pull on the concrete. The concrete shell roof was chosen because shell roofs are efficient civil engineering structures (Ramm, 2004).

A summary of the type of applied loads and the scaling factors α on all structures is depicted in Table 3.1:

Table 3.1: The type of loading and the scaling factors of the selected structures.

Structure	Type of loading	Scaling factor α
Steel truss	Point loads on all upper nodes in the z-direction	10
Critical steel beam	Compressive force in the beam's direction	10
Steel Vierendeel girder	Point loads on all upper nodes in the z-direction	10
Concrete two-way slab	Distributed load over the whole structure	10
Concrete shell roof	Distributed load over the whole structure	10

3.2. Conversion rules

This section is based on the conversion rules of P. Hoogenboom (2023). The conversion rules for modelling the small-scale and real-sized structures can be divided into three parts:

1. Conversion of dimensions
2. Conversion of material properties and supports
3. Conversion of loads

Conversion of dimensions

In this project, all small-scale structures are one-tenth of the size of the real-sized structure. The scaling factor α is left as a variable to obtain conversion rules applicable to all scaling factors. The conversion rules for the dimensions of a concrete shell are shown in Table 3.2.

Table 3.2: Converion rules for shell structures. All variables of the real-sized structure are a factor α larger than those in the small-scale structure.

Dimensions	Real-sized	Small-scale
Span	l	l/α
Radius of curvature	a	a/α
Thickness	t	t/α
Reinforcement diameter	d	d/α

For columns and beams, similar conversion rules apply. Table 3.3 shows the conversion rules for columns and beams.

Table 3.3: Conversion rules for columns and beams. All variables of the real-sized structure are a factor α larger than those in the small-scale structure.

Dimensions	Real-sized	Small-scale
Length	l	l/α
Width of cross-section	w	w/α
Height of cross-section	h	h/α

Conversion of material properties and supports

The relevant material properties are the following:

- The Young's modulus (E)
- The Poisson's ratio (ν)
- The yield strength (f)
- The mass density (ρ)

All these material properties are identical for both structures. Additionally, the damping of the real-sized structure and the stiffnesses do not change.

Conversion of loads

There are three types of loads: a distributed load p in kN/m^2, a line load q in kN/m and a point load P in kN. A distributed load does not change for the small-scale structure. A line load on the small-scale structure differs by a factor of $1/\alpha$ with the real-sized structure and a point load differs by a factor of $1/\alpha^2$. The gravitational acceleration stays the same in both structures.

Conclusions

The conversion rules follow general structural mechanics and the following can be concluded:

- The deflection in the real-sized structure is α times the small-scale structure.
- The stresses in both the small-scale and the real-sized structures are identical.
- The buckling length of the real-sized structure is α times the buckling length of the small-scale structure.
- The internal forces in beams and columns in the real-sized structure are α^2 times the forces in the small-scale structure.

4

Analysis of a Steel Truss

Steel trusses are used widely in civil engineering structures (Machacek & Cudejko, 2011). All forces are transferred by normal forces, which makes the beams susceptible to buckling. In the non-linear calculation, the focus is set on the imperfections of beams because buckling resistance decreases significantly when an imperfection is added to the beam.

There are two different models for both the small-scale and real-sized trusses. The first model has members with a bending stiffness and rigid connections. This model is prone to local buckling. The second model does not have any bending stiffness and can only buckle globally. There will be no bending in this truss. Both trusses are loaded with point loads on the upper nodes and have identical material en geometrical properties. The following common properties were chosen for the real-sized truss. The entire truss is made of S355 construction steel with a yield strength of 355 N/mm^2. All beams have a circular cross-sectional area with a diameter of 2.5 in (This particular cross-section was selected because, among the limited choices available to SCIA engineers, there was a small-scale diameter of 0.25 in, which is exactly 10 times smaller). Furthermore, the structure has a length of 6 m and a height of 1 m. In Figure 4.1, the model of the truss is depicted.

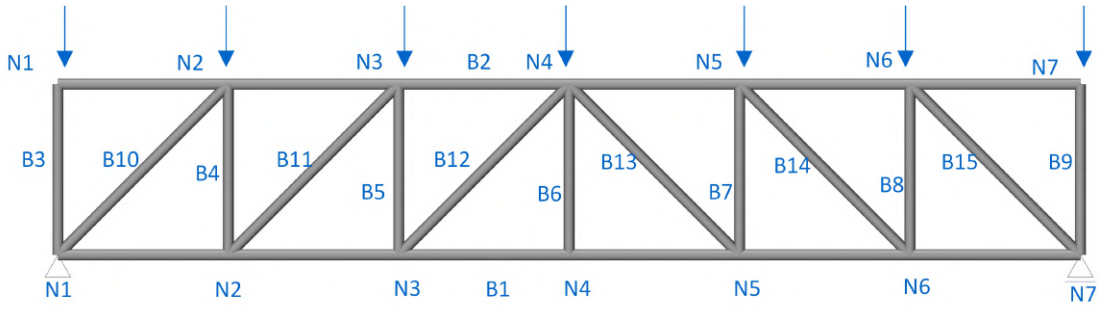

Figure 4.1: SCIA Engineer model of the steel truss with all members' names and node names.

The small-scaled truss has the same material properties as the real-sized one. However, its diameter is 0.25 in and its length and height are 0.6 m and 0.1 m respectively.

4.1. Steel truss with bending stiffness

This first model of the steel truss was subjected to point loads on all upper nodes ranging from 1 kN to 8 kN and 100 kN to 800 kN. First, a linear analysis was done. Second, a non-linear analysis was done with bow imperfections following the buckling data.

4.1.1. Moments and displacements with a linear calculation

To see how the structure would buckle, a linear stability analysis was done by SCIA Engineer. The applied point loads were 1 kN and 100 kN. Figures 4.2 and 4.3 show the linear buckling analysis for the small-scale and real-sized steel truss.

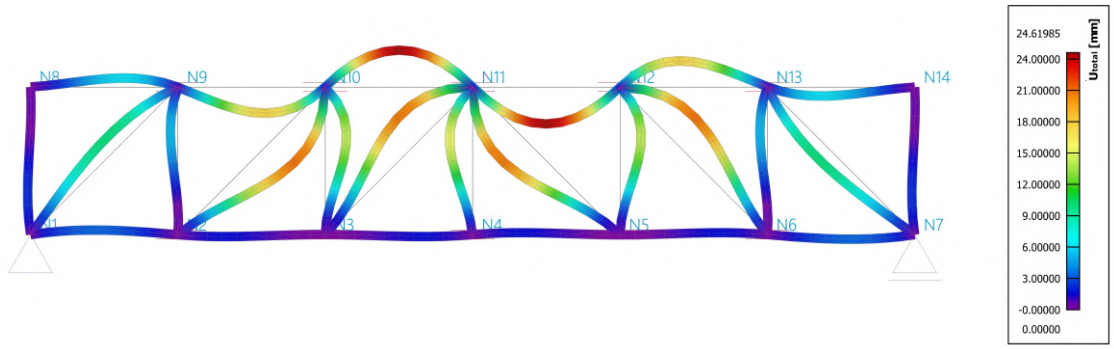

Figure 4.2: Linear stability analysis of the small-scale truss with bending stiffness when subjected to point loads of 1 kN.

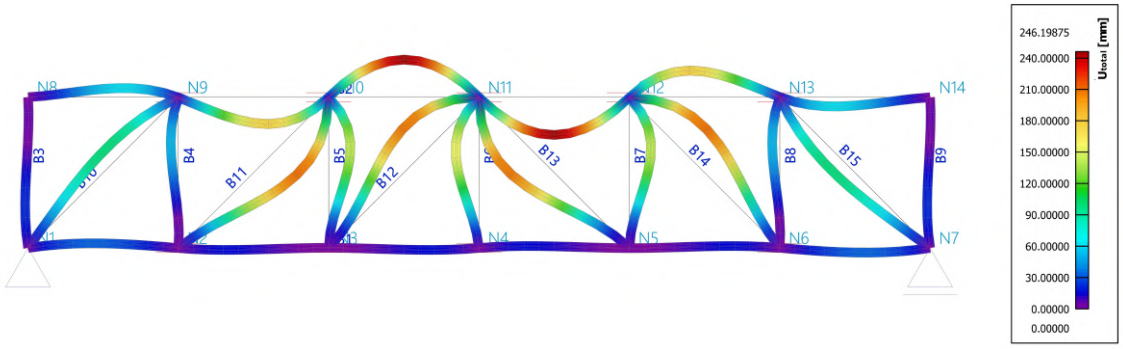

Figure 4.3: Linear stability analysis of the real-sized truss with bending stiffness when subjected to point loads of 100 kN.

The members in these trusses bend because the structure has a bending stiffness EI. Almost all members in the truss buckle. In this chapter, the focus is on member B10, because this is one of the longer beams in the truss and will buckle earlier according to Euler's buckling theory (Mukuvare, 2013). For the bending moments, node N4 will be the focus. This is in the middle of the truss. The moments are at a maximum here. Figure 4.4 shows the total displacement at the midspan of member B10 when subjected to loads ranging from 1 kN to 8 kN and 100 kN to 800 kN.

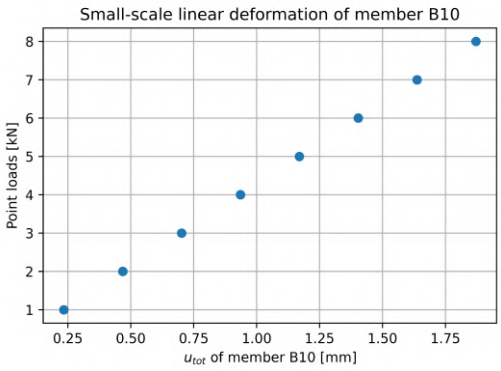

(a) Force-Displacement diagram of member B10 for the small-scale structure.

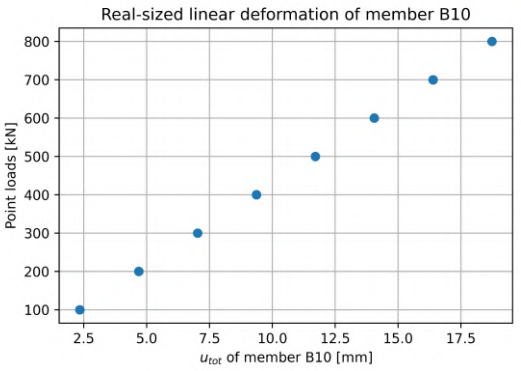

(b) Force-displacement diagram of member B10 for the real-sized structure.

Figure 4.4: Linear force-displacement graph of both the small-scale and real-sized truss. The displacement at the midspan of member B10 is depicted when subjected to point load ranging from 1 kN to 8 kN and 100 kN to 800 kN.

The displacements are all 10 times larger in the real-sized truss which is in line with the conversion rules. For visualisation purposes, Figures 4.5 and 4.6 show the displacement of the entire structures when subjected to loads of 8 kN and 800 kN.

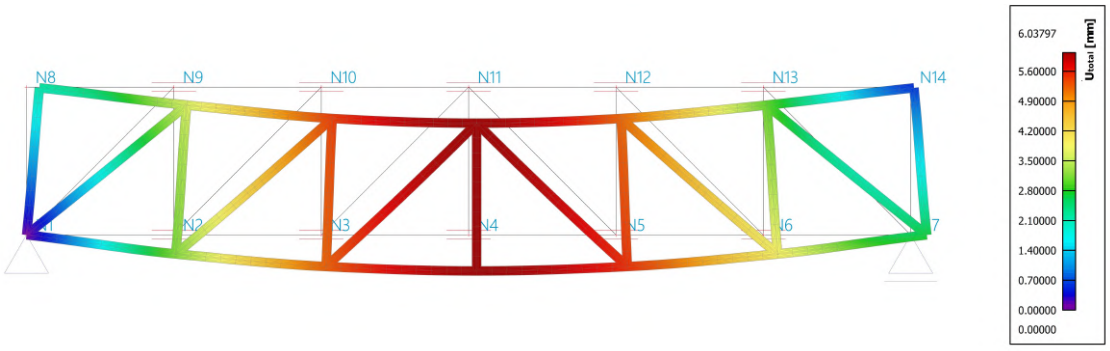

Figure 4.5: Linear deformation of the small-scale truss when subjected to point loads of 8 kN.

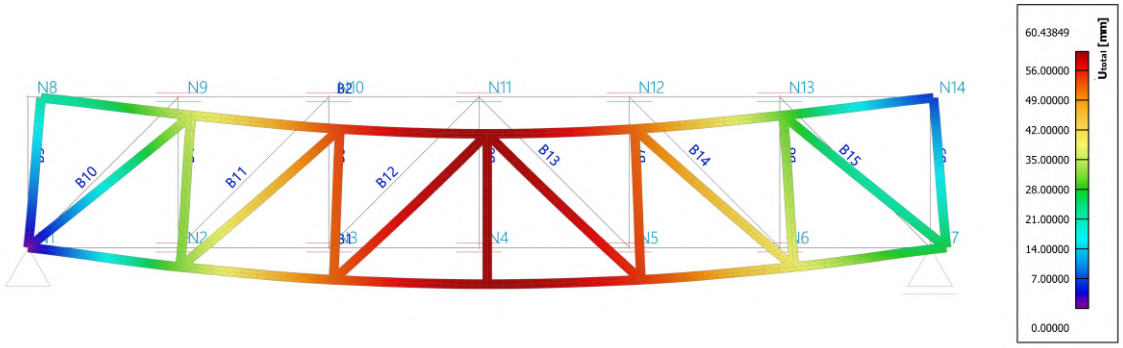

Figure 4.6: Linear deformation of the real-sized truss when subjected to point loads of 800 kN.

The maximum displacement of the real-sized truss is 60.44 mm and the small-scale truss deforms at a maximum of 6.04 mm, which is 10 times smaller than the deformation of the real-sized truss. This reaffirms the conversion rules for linear material behaviour. The moments at node N4 are analysed in addition to the displacements of member B10. The moments in the real-sized truss are 1000 times larger than the moments in the small-scale truss because the structure is subjected to point loads instead of a distributed load or line load. Figure 4.7 illustrates the moments of both structures when subjected to loads ranging from 1 kN to 8 kN and 100 kN to 800 kN.

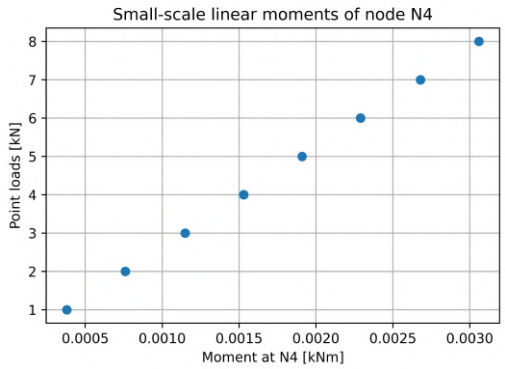

(a) Force-Moment diagram of node N4 for the small-scale structure.

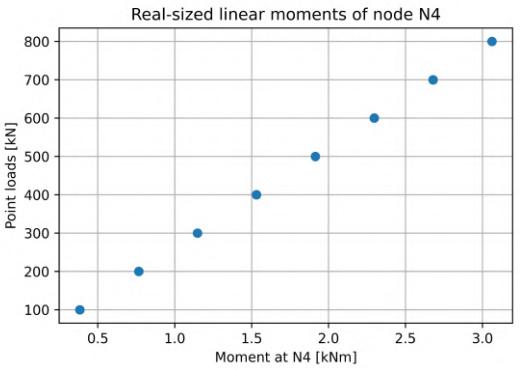

(b) Force-Moment diagram of node N4 for the real-sized structure.

Figure 4.7: Linear force-moment diagram of both the small-scale and real-sized truss. The moment at node N4 is depicted when subjected to point load ranging from 1 k to 8 kN and 100 kN to 800 kN.

The moments in the real-sized truss differ by a factor of 1000 from the moments in the small-scale truss. Therefore, the conversion rule also applies to moments.

4.1.2. Moments and displacements with a non-linear calculation

For the non-linear calculation, a bow imperfection was added to all beams in the truss, following the linear buckling data. Again, member B10 and node N4 were analysed to make a comparison between the linear and non-linear calculations. First, the non-linear displacements at midspan of member B10 are depicted in Figure 4.8 for both structures.

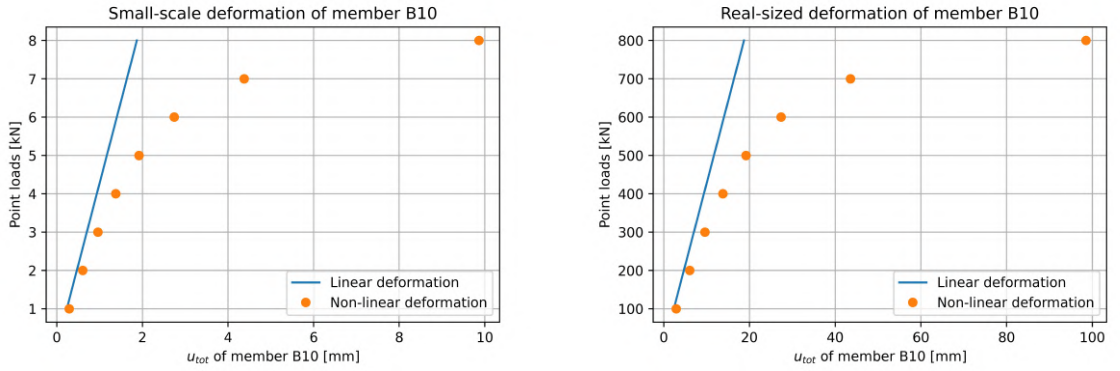

(a) Non-linear Force-Displacement diagram of member B10 for the small-scale structure.

(b) Non-linear Force-displacement diagram of member B10 for the real-sized structure.

Figure 4.8: Non-linear force-displacement graph of both the small-scale and real-sized truss. The displacement at midspan of member B10 is depicted when subjected to point load ranging from 1 k to 8 kN and 100 kN to 800 kN.

All non-linear deformations follow the conversion rules. The non-linear deformations in the small-scale truss are 10 times smaller than the deformations in the real-sized truss. The non-linear calculation also differs significantly from the linear calculation when the load increases. This shows the larger deformations as the structure is loaded more. Figures 4.9 and 4.10 illustrate the non-linear deformation of both structures when subjected to a load of 8 kN and 800 kN, respectively.

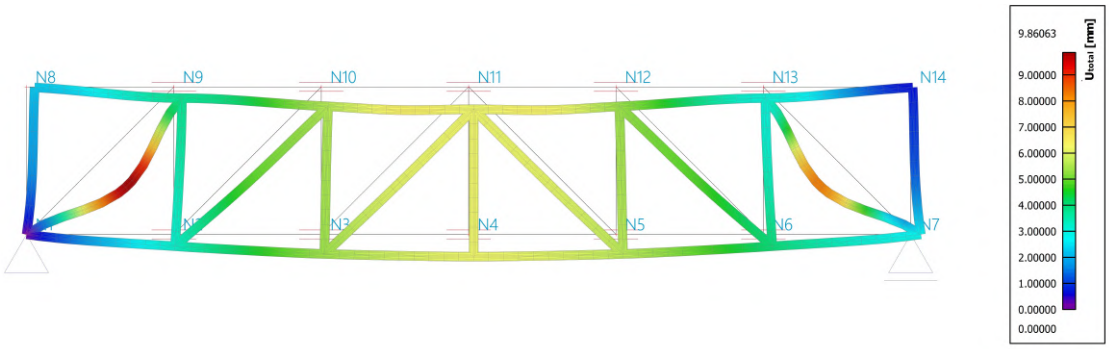

Figure 4.9: Non-linear displacement of the small-scale truss when subjected to a load of 8 kN.

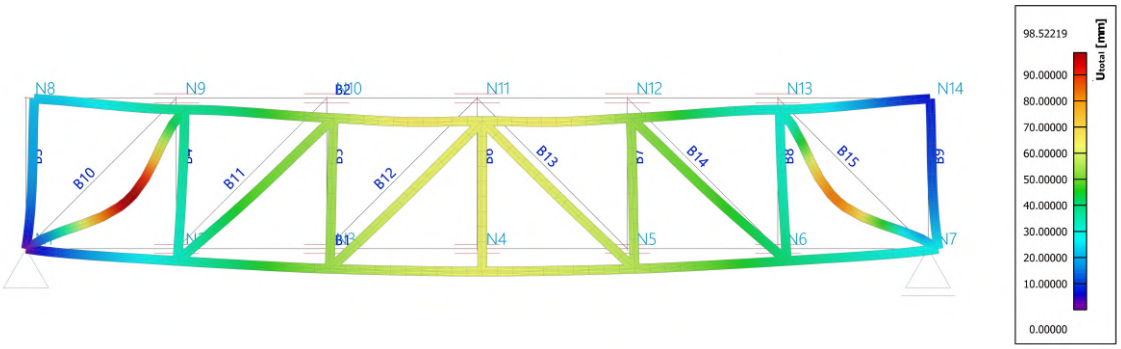

Figure 4.10: Non-linear displacement of the real-sized truss when subjected to a load of 800 kN.

Member B10 buckles in both structures and has the largest deformation. The maximum deformation of member B10 in the small-scale truss is 9.86 mm and the deformation of member B10 in the real-sized truss is 98.52 mm. The displacement in the real-sized truss is approximately 10 times larger than the displacement in the small-scale truss. The small difference is a numerical error SCIA Engineer makes in a non-linear calculation.

Similarly, the non-linear moments are analysed. Figure 4.11 illustrates the linear and non-linear moments of node N4 for both the small-scale and real-sized truss.

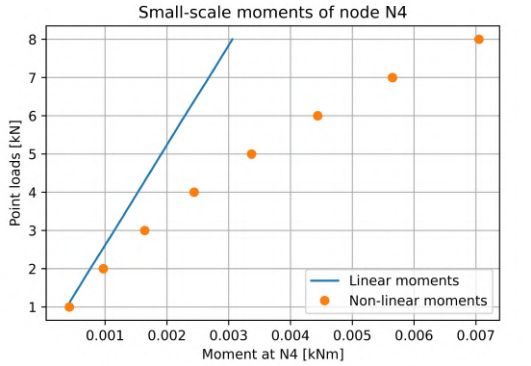

(a) Non-linear force-moment diagram of node N4 for the small-scale structure.

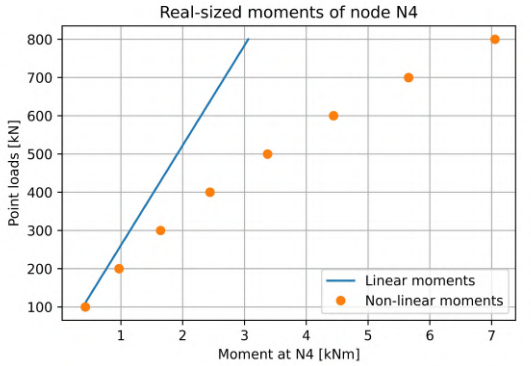

(b) Non-linear force-moment diagram of node N4 for the real-sized structure.

Figure 4.11: Non-linear force-moment diagram of both the small-scale and real-sized truss. The moment at node N4 is depicted when subjected to point load ranging from 1 kN to 8 kN and 100 kN to 800 kN.

The moments in the real-sized structure differ by a factor of 1000 from the moments in the small-scale structure. Therefore, the conversion rules still apply for moments when computed with a non-linear calculation.

4.2. Steel truss without bending stiffness

The second model of the steel truss is modelled without taking bending stiffness into account. Therefore, the members cannot bend. They can only elongate or shrink, which means that the only internal forces are normal forces. This section will therefore focus on normal forces and nodal displacements. Nodal displacements are chosen because the displacement is not a function of the length of the beam. Furthermore, this system has global buckling. Therefore, there are not any buckling imperfections in the non-linear calculation, but rather global buckling imperfections following a linear stability analysis.

4.2.1. Normal forces and displacements with a linear calculation

First, the normal forces in all members are tabulated when subjected to point loads of 210 kN and 21000 kN on the upper nodes of the truss. Similarly, the displacements of all nodes are tabulated.

Second, normal forces in member B10 and displacements of node N4 are plotted when subjected to point loads ranging from 100 kN to 210 kN and 1000 kN to 21000 kN. Table 4.1 depicts the normal forces computed with a linear calculation for both structures. The applied loads are 210 kN and 21000 kN.

Table 4.1: Linear normal forces for all members in the structures when subjected to point loads of 210 kN and 21000 kN. The factor between the point loads is also depicted.

Name	N [kN]		
	Small-scale	Real-sized	Factor
B1	525	52500	100
B2	0	0	-
B3	-210	-21000	100
B4	315	31500	100
B5	105	10500	100
B6	0	0	-
B7	105	10500	100
B8	315	31500	100
B9	-210	-21000	100
B10	-742	-74246	100
B11	-445	-44548	100
B12	-148	-14849	100
B13	-148	-14849	100
B14	-445	-44548	100
B15	-742	-74246	100

The normal forces differ by a factor of 100 in all members of the truss, which is in line with the conversion rules. The nodal displacements of all members are depicted in Table 4.2.

Table 4.2: Horizontal, vertical and total displacements of all nodes of both structures when subjected to point loads of 210 kN and 21000 kN computed with a linear calculation.

Name	u_x [mm]		u_z [mm]		Factors	
Small-scale	Real-sized	Small-scale	Real-sized	Small-scale	u_x	u_z
N1	0.000000	0.00000	-0.000008	-0.000080	-	10.0000
N2	7.886435	78.94156	-82.243122	-823.236290	10.0098	10.0098
N3	20.504730	205.24800	-136.636302	-1367.701100	10.0098	10.0098
N4	34.700319	347.34279	-155.293107	-1554.451900	10.0098	10.0098
N5	48.895899	489.43761	-136.636302	-1367.701100	10.0098	10.0098
N6	61.514199	615.74411	-82.243122	-823.236290	10.0098	10.0098
N7	69.400631	694.68570	-0.000008	-0.000080	10.0098	10.0000
N8	55.205051	552.59091	-3.154582	-31.576700	10.0098	10.0098
N9	55.205051	552.59091	-77.511273	-775.871400	10.0098	10.0098
N10	47.318611	473.64929	-135.058999	-1351.912000	10.0098	10.0098
N11	34.700319	347.34279	-155.293107	-1554.451900	10.0098	10.0098
N12	22.082020	221.03640	-135.058999	-1351.912000	10.0098	10.0098
N13	14.195580	142.09481	-77.511273	-775.871400	10.0098	10.0098
N14	14.195580	142.09481	-3.154582	-31.576700	10.0098	10.0098

The displacements differ by a factor 10, which is in line with the conversion rules. For visualisation purposes, the deformation of both structures is illustrated in Figures 4.12 and 4.13 when subjected to point loads of 210 kN and 21000 kN.

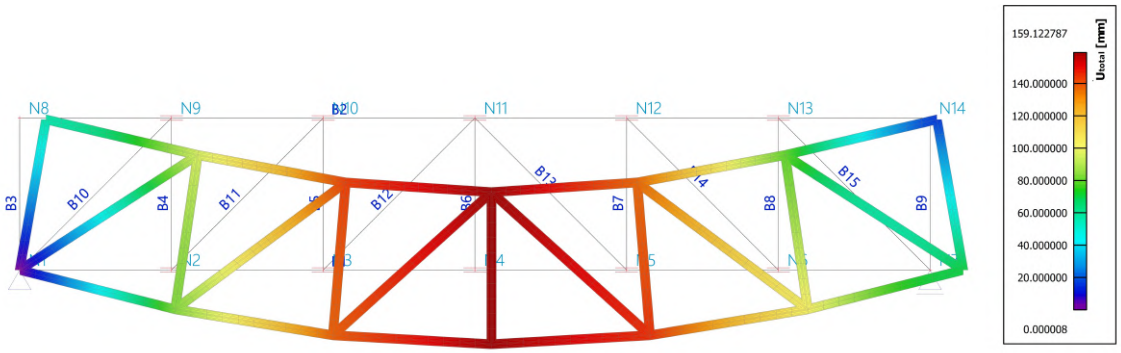

Figure 4.12: Linear deformation of the small-scale truss when subjected to point loads of 210 kN.

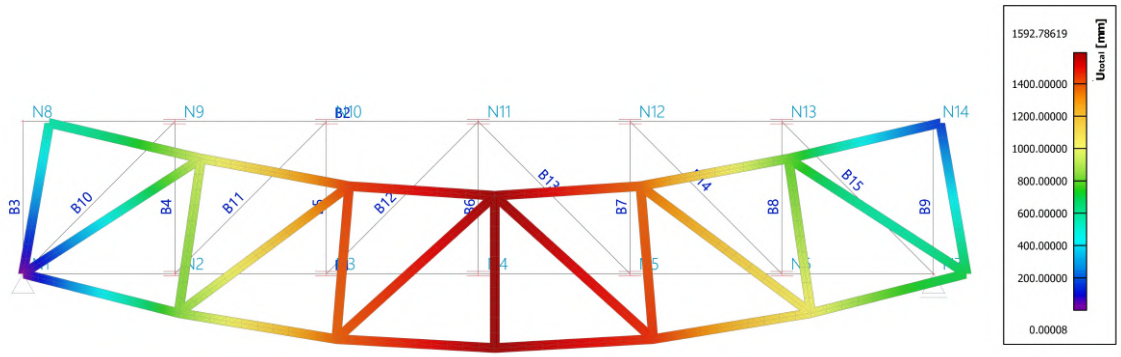

Figure 4.13: Linear deformation of the real-sized truss when subjected to point loads of 21000 kN.

Figures 4.12 and 4.13 illustrate the absence of bending stiffness in this second model. The beams do not bend. They are only translated and rotated. For the global buckling shape, a linear buckling analysis was done. Figures 4.14 and 4.15 illustrate the buckling shape of the small-scale and real-sized structures, respectively. The applied point loads are 10 kN for the small-scale truss and 1000 kN for the real-sized truss.

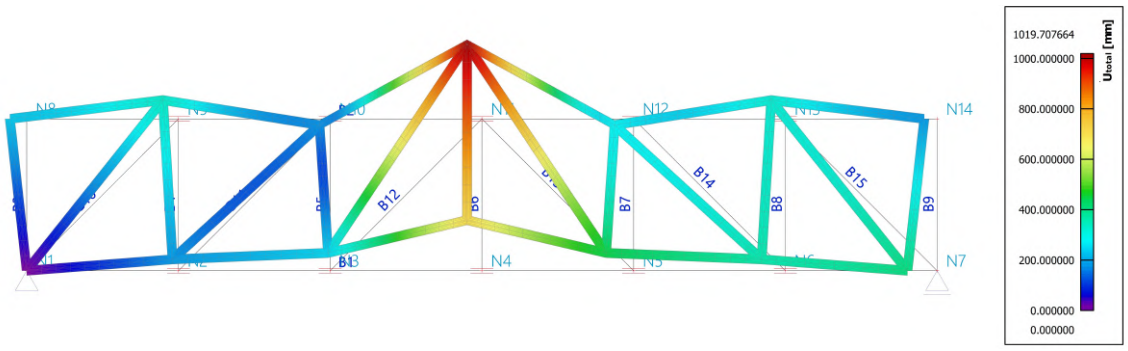

Figure 4.14: Linear buckling analysis of the small-scale structure when subjected to point loads of 10 kN.

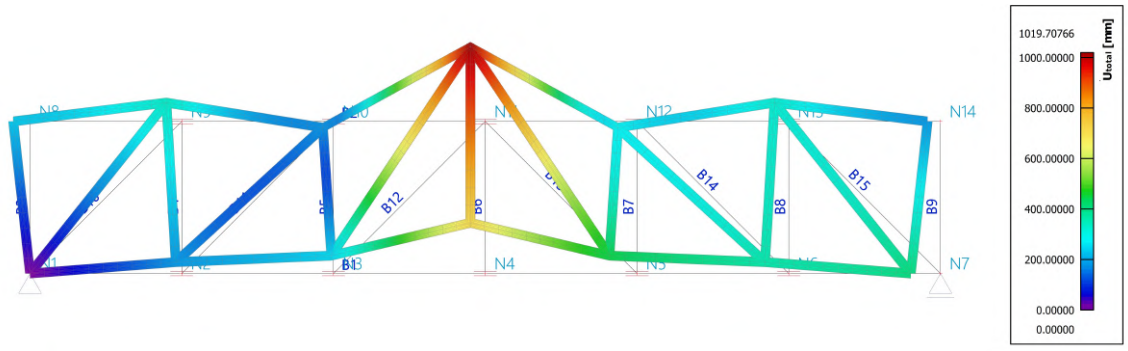

Figure 4.15: Linear buckling analysis of the real-sized structure when subjected to point loads of 1000 kN.

The stability analysis shows that the beams will not buckle. Only the global systems buckle. Furthermore, figures 4.16 and 4.17 illustrate the displacements of node N4 and the normal force in member B10 respectively. The applied point loads range from 10 kN to 210 kN and 1000 kN to 21000 kN.

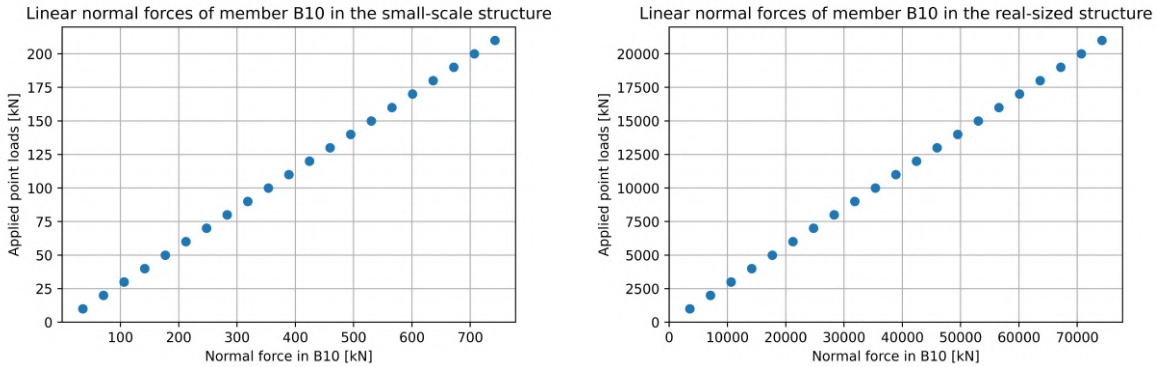

(a) Normal forces in member B10 of the small-scale structure. **(b)** Normal forces in member B10 of the real-sized structure.

Figure 4.16: Applied point loads vs normal forces at member B10 of both the small-scale and real-sized structure. The applied point loads range from 10 kN to 210 kN and 1000 kN to 21000 kN.

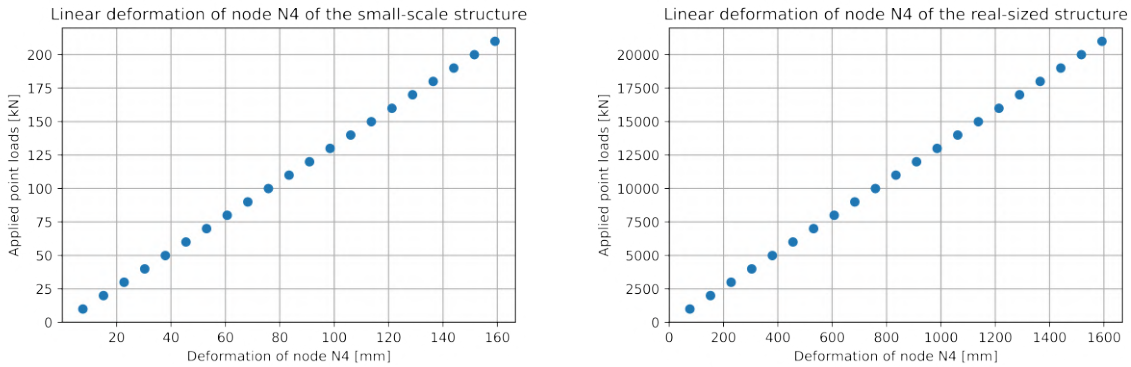

(a) Displacement of node N4 of the small-scale structure. **(b)** Displacement of node N4 of the real-sized structure.

Figure 4.17: Applied point loads vs displacements at node N4 of both the small-scale and real-sized structure. The applied point loads range from 10 kN to 210 kN and 1000 kN to 21000 kN.

Figures 4.16 and 4.17 reaffirm the conversion rules for the other applied point loads. Namely, the moments differ by a factor of 100 and the displacements by a factor of 10.

4.2.2. Normal forces and displacements with a non-linear calculation

The non-linear calculations in the steel truss without bending stiffness were done with a global imperfection. This global imperfection is an additional displacement of 10 mm on the members of the real-sized structure and 1 mm on the members of the small-scale structure. Again, the focus lies on the normal forces in member B10 and the displacement of node N4. Table 4.3 depicts the non-linear normal forces in all members when the applied point loads are 210 kN and 21000 kN respectively.

Table 4.3: Non-linear normal forces in both the small-scale and real-sized trusses when subjected to point loads of 210 kN and 21000 kN.

Name	N [kN]		
	Small-scale	Real-sized	Factor
B1	641.97	64202.43	100.01
B2	-90.19	-9020.80	100.02
B3	-145.2	-14521.49	99.98
B4	155.13	15514.04	100.01
B5	-200.4	-20043.29	100.04
B6	-405.8	-40614.00	100.09
B7	-200.4	-20043.29	100.04
B8	155.13	15514.04	100.01
B9	-145.2	-14521.49	99.98
B10	-469.3	-46930.13	100.00
B11	-368.2	-36806.79	99.96
B12	-192.2	-19225.43	100.05
B13	-192.2	-19225.43	100.05
B14	-368.2	-36806.79	99.96
B15	-469.3	-46930.13	100.00

The factors are all around 100, which means that the conversion rule applies. The small numerical errors are negligible. Similarly, the displacements for these load cases are depicted in Table 4.4.

Table 4.4: Non-linear nodal displacements in both the small-scale and real-sized trusses when subjected to point loads of 210 kN and 21000 kN.

Name	u_x [mm]		u_z [mm]		Factors	
Small-scale	Small-scale	Real-sized	Small-scale	Real-sized	u_x	u_z
N1	0.00000	0.000000	-0.000008	-0.00008	-	10.0000
N2	10.05721	100.679400	-81.826121	-819.09442	10.0107	10.0102
N3	24.56034	245.845200	-137.322610	-1374.58301	10.0098	10.0099
N4	42.40226	424.468100	-154.798810	-1549.51799	10.0105	10.0099
N5	60.24417	603.091000	-137.322610	-1374.58301	10.0108	10.0099
N6	74.74730	748.256800	-81.826121	-819.09442	10.0105	10.0102
N7	84.80452	848.936200	-0.000008	-0.00008	10.0105	10.0000
N8	66.87737	669.460770	-1.802039	-18.03437	10.0103	10.0078
N9	65.94274	660.103080	-79.260588	-793.41179	10.0102	10.0102
N10	57.80629	578.670620	-140.260400	-1404.00195	10.0105	10.0100
N11	42.40226	424.468100	-160.895900	-1610.60596	10.0105	10.0102
N12	26.99822	270.265610	-140.260400	-1404.00195	10.0105	10.0100
N13	18.86177	188.833000	-79.260588	-793.41179	10.0114	10.0102
N14	17.92714	179.475290	-1.802039	-18.03437	10.0114	10.0078

The displacements in the small-scale structure are 10 times smaller than the displacements in the real-sized structure, which is in line with the conversion rules. Additionally, Figures 4.18 and 4.19 illustrate the deformed structures when subjected to point loads of 210 kN and 21000 kN computed with a non-linear calculation.

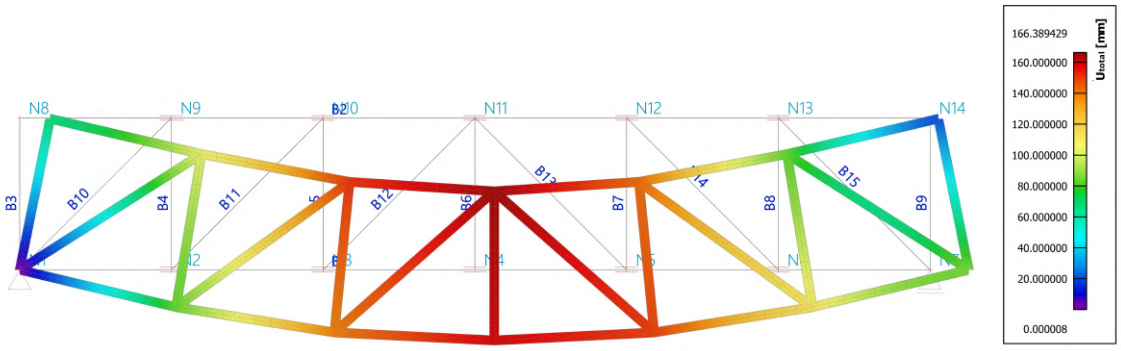

Figure 4.18: Non-linear deformation of the small-scale truss when subjected to point loads of 210 kN.

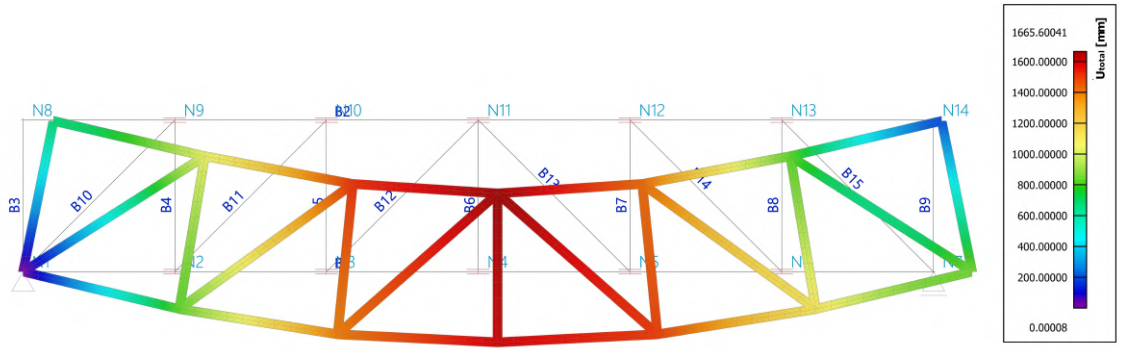

Figure 4.19: Non-linear deformation of the real-sized truss when subjected to point loads of 21000 kN.

Figures 4.18 and 4.19 reaffirm the conversion rule for displacements. The maximum displacement in the small-scale truss is 166.4 mm and the maximum displacement in the real-sized truss is 1665.6 mm.

In comparison with the linear analysis, point loads ranging from 10 kN to 210 kN and 1000 kN to 21000 kN were analysed with a non-linear calculation. Again, the normal forces and displacements were computed. Figures 4.20 and 4.21 illustrate the normal forces in member B10 and displacements of node N4 respectively.

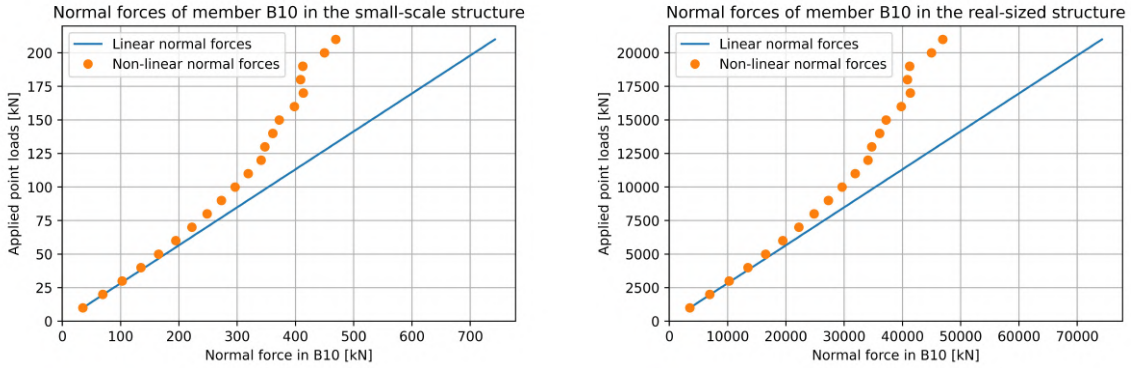

(a) Normal forces in member B10 of the small-scale structure. **(b)** Normal forces in member B10 of the real-sized structure.

Figure 4.20: Applied point loads vs normal forces in member B10 of the small-scale and real-sized structure. The applied point loads range from 10 kN to 210 kN and 1000 kN to 21000 kN.

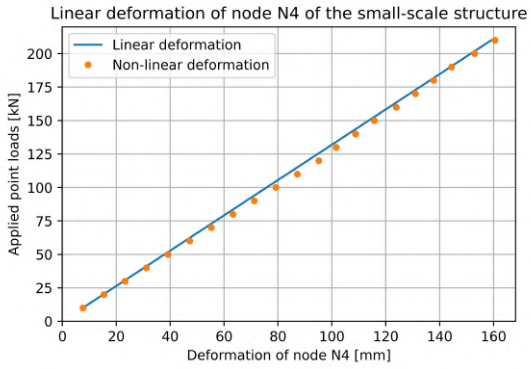

(a) Non-linear displacement of node N4 of the small-scale structure.

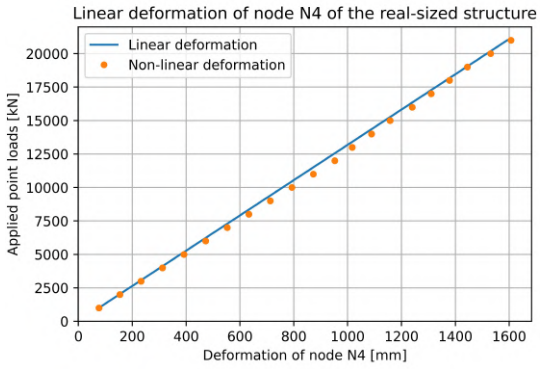

(b) Non-linear displacement of node N4 of the real-sized structure.

Figure 4.21: Applied point loads vs displacements of node N4 of both the small-scale and real-sized structure. The applied point loads range from 10 kN to 210 kN and 1000 kN to 21000 kN.

The non-linear normal forces in member B10 are larger than the linear normal forces. The irregularity in the non-linear forces happens because the structure divides the forces over the members differently per applied load. Namely, the structures have relatively large displacements. The members on the bottom of the truss will have large tensile forces. Therefore, the horizontal component of the force in member B10 will decrease. This is exactly what is seen in Figure 4.20. However, the same irregularity is seen in both structures, which means that the conversion rules apply. Namely, the normal forces in the real-sized structure are 100 times larger than the normal forces in the small-scale structure.

Furthermore, the non-linear displacements of node N4 do not differ much from the linear displacements. This happens because the structure is only subjected to global buckling instead of local buckling. However, the non-linear displacements in the small-scale structure are 10 times smaller than the displacements in the real-sized structure, which is in line with the conversion rule for displacements.

5
Analysis of a Steel Beam

In practice, all structures have initial geometrical imperfections. Therefore, these imperfections are modelled in SCIA Engineer for the critical beam of the steel truss in Chapter 4. For both the small-scaled and real-sized structures, the members have an imperfection following the buckling pattern. The pattern follows a sinusoidal pattern and was discovered by the mathematician Leonhard Euler. His formula for the buckling force follows in Equation 5.1:

$$F_{buc} = \frac{\pi^2 EI}{l_{buc}^2}, \tag{5.1}$$

where EI is the bending stiffness in KNm^2 and l_{buc} is the buckling length which depends on the boundary conditions of the member (Mukuvare, 2013). These imperfections decrease the maximal allowable buckling force significantly. Therefore, columns will always have a safety factor for buckling forces defined by the Eurocode (Welleman, n.d.). Chapter 5 is subdivided into the following three parts to analyse the non-linear material behaviour extensively:

- Finding the critical beam in the truss for the buckling force using the method described in the Eurocode (Welleman, n.d.).
- Modelling this beam in SCIA engineer and then subjecting it to buckling imperfections.
- Computing nodal moments and moments at midspan for a statically indeterminate beam using the method described in the Eurocode and SCIA Engineer.

5.1. Maximum buckling force for the critical beam using the Eurocode

The critical beams for buckling are the inclined members in the truss. Equation 5.1 demonstrates that the inclined members will have reduced resistance to buckling because of their greater length. The other variables are identical for all members. The method that will be used to compute their buckling strength is described in Eurocode 1993-1-1 (Welleman, n.d.). An elaborate explanation of the method is shown in Appendix B. Furthermore, $\bar{\lambda}$ is the relative slenderness. It is a unitless parameter. ϕ and χ are safety factors. All relevant safety factors and the final buckling resistances of both structures are depicted in Table 5.1.

Table 5.1: All relevant buckling data and the final buckling resistance of both structures according to Eurocode 1993-1-1. The buckling resistance is compared and is depicted in the last row.

Parameter	Small-scaled structure	Real-sized structure
A $[mm^2]$	31.66921744	3166.922
λ $[-]$	1.165885552	1.165886
ϕ $[-]$	1.41628652	1.416287
χ $[-]$	0.450371838	0.450372
N_{bRd} [kN]	**5.063337903**	**506.3338**

The buckling resistance of the small-scaled structure is exactly one-tenth of the real-sized structure. Therefore, it can be concluded that the Eurocode adheres to conversion rules when determining the

buckling resistance of a column. This is apparent as the Eurocode employs a safety factor based on the material's strength, which, in this instance, was S355 construction steel for both materials.

5.2. Maximum buckling force for the critical beam with finite element analysis

The critical beams in the structures are modelled separately in SCIA engineer. These beams have the same cross-sectional and material properties as the steel truss. The model is illustrated in Figure 5.1.

Figure 5.1: Modelled beam in SCIA engineer. This is one of the inclined members in the truss and has the critical buckling resistance

Both the small-scaled beam and the real-sized beam will be subjected to their maximum allowable buckling force. This force is computed with Equation 5.1 and is 8.27 kN and 827 kN respectively. To observe non-linear results, both structures will be subjected to this critical buckling force. Then, a non-linear calculation is performed and the results are shown in Table 5.2.

Table 5.2: Displacements at midspan of both the small-scaled structure and the real-sized structure when subjected to their maximal buckling force.

	u_x [mm]	u_z [mm]	U_{total} [mm]
Small-scale beam	-0.08791	2.82686	2.82822
Real-sized beam	-0.87946	28.25405	28.26773
Factor	10.00	9.995	9.995

When both beams are subjected to their critical buckling force, the conversion rules do apply in this case. The force applied on the real-sized is one-hundredth of the force applied on the small-scale structure. As a result, the displacements in the x- and y-directions differ by a factor of 10.

A second method involves applying a force equivalent to 90% of the buckling resistance. This is done because this force will likely be in the non-linear curve of the buckling force curve which might give different results as expected. The forces applied to the structures will be 744.3 kN and 7.443 kN. The displacements at midspan as a result of these forces are depicted in Table 5.3.

Table 5.3: Displacements at midspan for both the small-scaled structure as the real-sized structure when subjected to a force of 7.443 kN and 744.3 kN respectively. This force is 90% of the critical buckling force.

	u_x [mm]	u_z [mm]	U_{total} [mm]
Small-scale beam	-0.079	1.67933	1.6812
Real-sized beam	-0.791	16.78898	16.8076
Factor	10.01	9.997	9.997

It can be concluded again that the displacements in the small-scaled structure are one-tenth of the real-sized structure. There are only marginal errors which can be explained by computational errors of the finite element analysis.

The results obtained in Tables 5.2 and 5.3 are not sufficient to make a Force-displacement diagram. Therefore, more forces are applied to the structure and the resultant Force-Displacement diagram is illustrated in Figure 5.2.

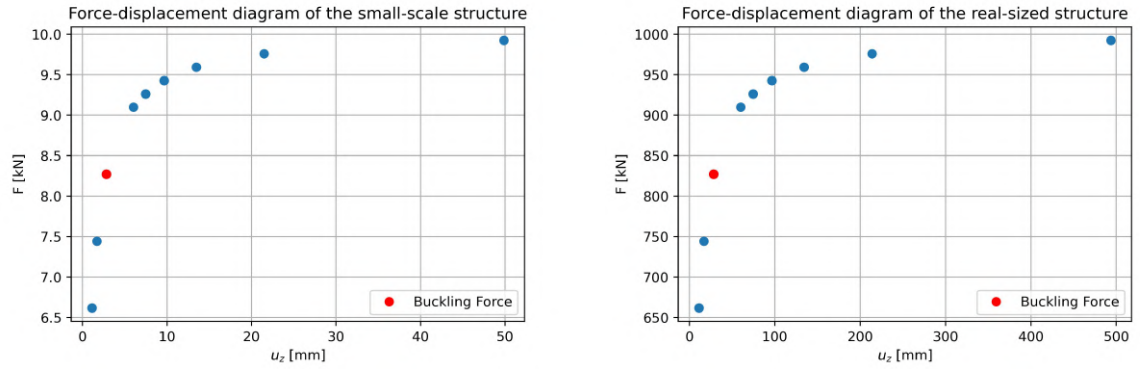

(a) Force-Displacement diagram of the small-scale beam.

(b) Force-Displacement diagram of the real-sized beam.

Figure 5.2: Force-displacement diagram for both the small-scale beam 5.2a and the real-sized beam 5.2b. The red dot shows the buckling force and the corresponding displacement. All data was retrieved from a non-linear SCIA Engineer calculation.

The Euler buckling force is illustrated in red in Subfigures 5.2a and 5.2b. For forces lower than this buckling resistance, both diagrams behave linearly. Forces larger than the buckling resistance result in very large displacements, thus geometric nonlinear material behaviour. However, the conversion rules still apply. Both graphs have the same shape and all factors differ by a factor of 100. The numerical values of these plots are depicted in Appendix A. Figures 5.3 and 5.3 show the displacement of the small-scale and real-sized beam when subjected to a compressive force of 9.924 kN and 992.4 kN, respectively.

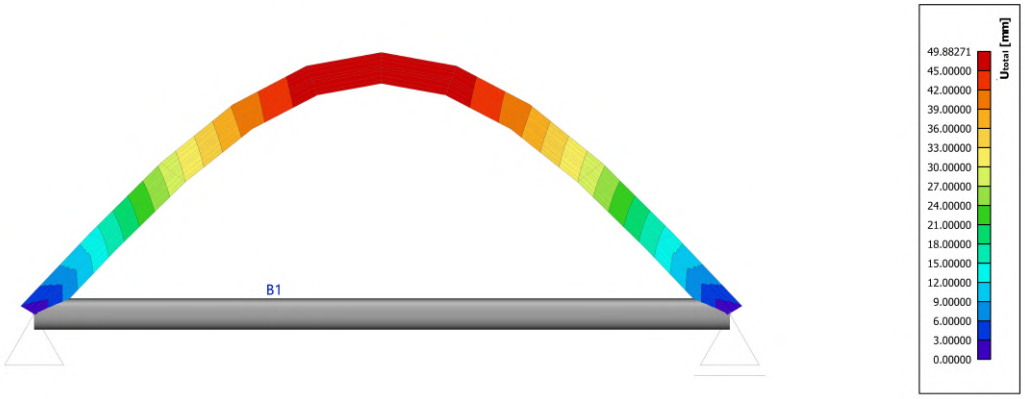

Figure 5.3: Deformation of the small-scale beam with a non-linear calculation when subjected to a compressive force of 9.924 kN.

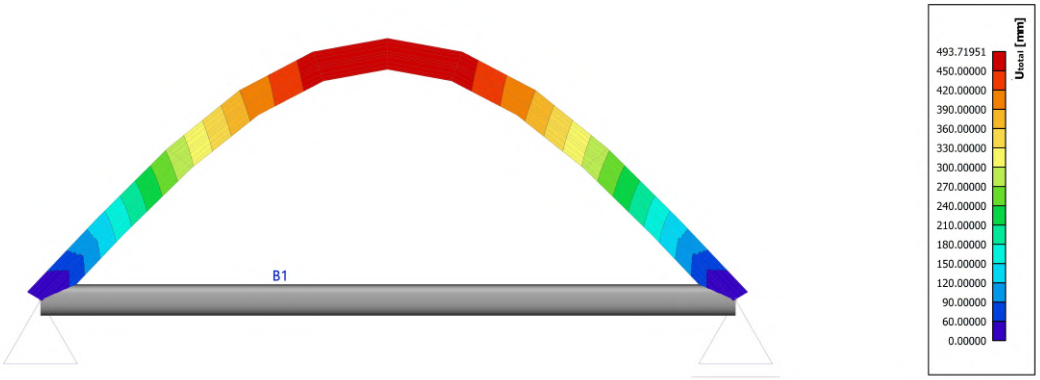

Figure 5.4: Deformation of the real-sized beam with a non-linear calculation when subjected to a compressive force of 992.4 kN.

The maximum displacement occurs at the midspan, which is 49.88 mm for the small-scale beam and 493.72 mm for the real-sized beam, which is in line with the conversion rules.

5.3. Physical non-linearity of a statically indeterminate beam

A statically indeterminate structure has more unknown reaction forces than equilibrium equations, which means that the structure's stiffness will be a variable in the problem (Zavatsky, n.d.). The boundary conditions of the structure in Figure 5.1 change to fixed supports, which will result in moments and no rotation in the supports. Furthermore, this beam has the same geometrical properties as the beam illustrated in Figure 5.1. Figure 5.5 illustrates the new boundary conditions of this critical beam.

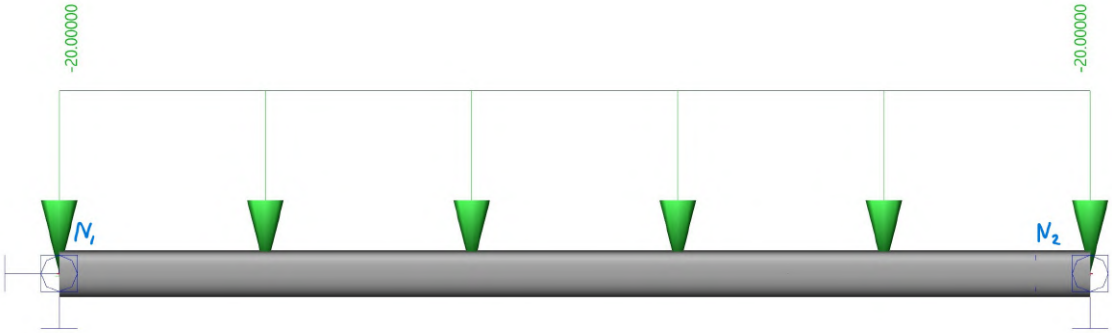

Figure 5.5: Statically indeterminate beam. The boundary conditions of the critical buckling beam have been changed to two fixed supports, which restrain rotation and displacement of the nodes.

Physical non-linearity is explained in Subsection 2.2.2. A structure exhibits physical non-linear material behaviour when it is subjected to a force yielding higher stresses than the yield strength. The structure has a relatively large buckling resistance due to the stiffer boundary conditions. Therefore, it is not interesting to apply a compressive force on the nodes, but rather apply a line load q in kN/m on the entire member. First, the moment at midspan and the nodal moments are computed with a hand calculation. This is done for both the small-scale and the real-sized statically indeterminate beam. Second, the structures are assessed by SCIA Engineer and finally, a conclusion is drawn.

5.3.1. Physical non-linear hand calculation using Eurocode 3

This statically indeterminate beam can be assessed in two ways. First, the general fourth-order differential equation, described in Equation 5.2, can be used, or an easier approach using the so-called force method (Hartsuijker, 2013). The fourth-order differential equation is as follows:

$$EI\frac{d^4w}{dx^4} = q, \tag{5.2}$$

where EI is the bending stiffness, w is the displacement, x is the axis along the length of the beam and q is the applied line load. Integrating Equation 5.2 gives expressions for the moment, shear force, rotation and curvature. However, an easier method can be used involving boundary conditions. Nodes N1 and N2 cannot rotate and symmetry shows that the moment in node N1 is identical to the moment in N2. The force method uses these boundary conditions as follows:

1. Add a hinge to the fixed support. Allow rotation around the y-axis in this case.
2. Compute the rotation using simple forget-me-nots (Welleman, n.d.). These are simple examples which have been computed using the fourth-order differential equation in Equation 5.2.
3. The rotations are zero, so the equation to solve for becomes $\phi = 0$. This will give the nodal moments

The statically indeterminate beam is reduced to a simply supported beam with two acting moments in the nodes M_1 and M_2. The rotation of node N1 follows in Equation 5.3:

$$\phi = \frac{M_1 l}{3EI} + \frac{M_2 l}{6EI} - \frac{ql^3}{24EI} \tag{5.3}$$

As was mentioned before, The moments M_1 and M_2 are identical. The expression in Equation 5.3 can be reduced and set equal to zero. This follows in Equation 5.4:

$$\begin{aligned} \phi &= \frac{Ml}{2EI} - \frac{ql^3}{24EI} = 0 \\ \Rightarrow M &= \frac{1}{12} ql^2 \end{aligned} \tag{5.4}$$

The moments at midspan can then be computed using the superposition of the moment due to the applied point load. This moment is $M_{mid} = \frac{1}{24} ql^2$. The moment line of this beam is illustrated in Figure 5.6. The chosen line load for this plot has a magnitude of 50 kN/m.

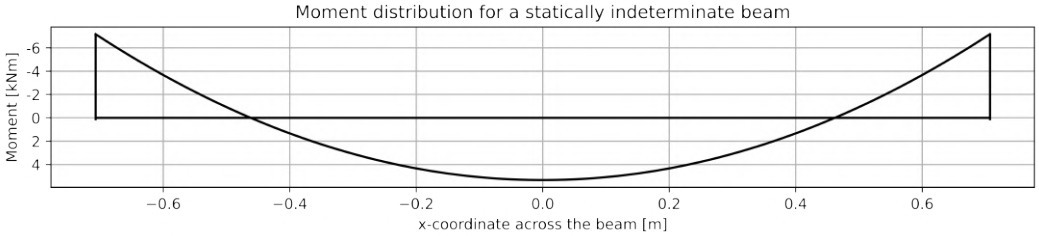

Figure 5.6: The moment diagram of the statically indeterminate beam. The chosen load was 50 kN/m^2.

The moments in the boundary conditions cannot become higher than the plastic moment capacity. The boundary condition will lose stiffness when this happens and the structure can become a mechanism. This plastic moment capacity can be computed using Eurocode 3. The formula for the plastic moment capacity is described in Equation 5.5

$$M_{pl,y,d} = \frac{W_{pl,y} f_y}{\gamma_{M0}} \tag{5.5}$$

where $W_{pl,y}$ is the section modulus in mm^3, f_y is the yield strength in N/mm^2 and γ_{M0} is a safety factor of 1 (Nemetschek Scia, 2014). The plastic moment capacities for the small-scale and real-sized truss follow in Equation 5.6:

$$\begin{aligned} M_{pl,y,d,RS} &= \frac{42675 \cdot 355}{1 \cdot 10^6} = 15.15\ kNm \\ M_{pl,y,d,SS} &= \frac{42.675 \cdot 355}{1 \cdot 10^6} = 0.0152\ kNm \end{aligned} \tag{5.6}$$

The real-sized and small-scale beams are subjected to relatively large line loads of 250 kN/m and 25 kN/m respectively. The moments at the hinges of both structures cannot exceed 15.15 kNm and 0.0152 kNm. The failure load of the statically indeterminate beam is computed as follows:

1. Compute the plastic moment capacity of the structure
2. Place hinges at the supports and midspan. Three hinges result in a mechanism.
3. Apply a virtual displacement or rotation
4. Compute the magnitude of the line load using the virtual work principle.

The derivation of this method is depicted in Appendix C. However, this is the total failure of the mechanism. The hinges at the supports fail earlier, namely at a failure load of $\frac{12M_{pl}}{l^2}$ instead of $\frac{16M_{pl}}{l^2}$. The failure loads of the small-scale and real-sized structures are depicted in Table 5.4.

Table 5.4: Failure load for the real-sized and small-scale statically indeterminate beam.

	Failure load of the supports [kN/m]	**Final failure load [kN/m]**
Real-sized structure	90.90	121.2
Small-scale structure	9.09	12.1

The conversion rules apply to this physical non-linear method. The plastic moment is reached at both nodes and midspan. Increasing the load further results in a mechanism and the moment at midspan will increase and the nodal moments will decrease.

5.3.2. Physical non-linear calculation using SCIA Engineer

The chosen physical non-linearity is the plasticity of the hinges. The small-scale and real-sized beams were subjected to line loads ranging from 2 kN/m to 20 kN/m and 20 kN/m to 200 kN/m with stepsizes of 2 kN/m and 20 kN/m. Additionally, the failure loads of 12.1 kN/m and 121.2 kN/m were analysed. The moments at midspan of the small-scale and real-sized structure are illustrated in Figure 5.7. Both linear and non-linear calculations were done. The failure load is also depicted.

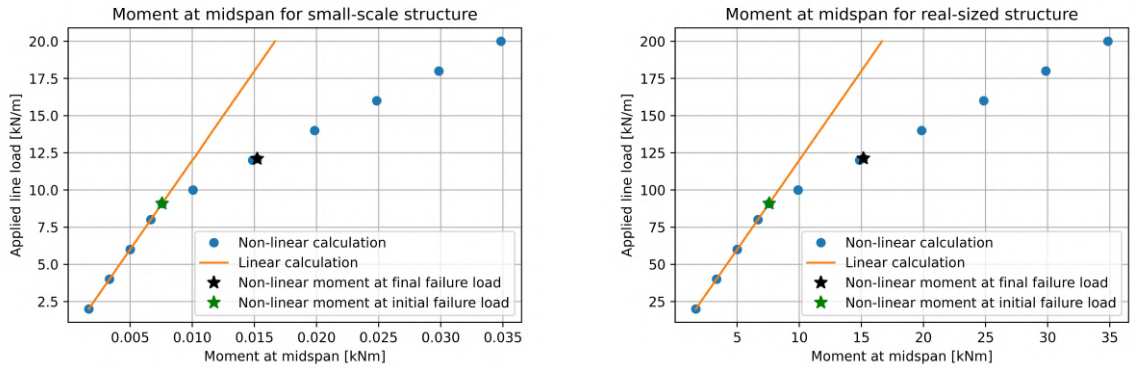

(a) Force-Moment diagram of the small-scale beam.

(b) Force-Moment diagram of the real-sized beam.

Figure 5.7: Force-Moment diagram for both the small-scale beam 5.7a and the real-sized beam 5.7b. Both the linear and non-linear calculation are depicted.

The behaviour of both structures changes when the failure load is reached. The moment at midspan will then increase at a lower rate. However, the second part of the curve still looks linear, which means that there is a bi-linear relation between the moment at midspan and the applied line load. The conversion rules do apply as Figure 5.7 shows. In addition, the nodal moments are assessed and similar diagrams follow in Figure 5.8.

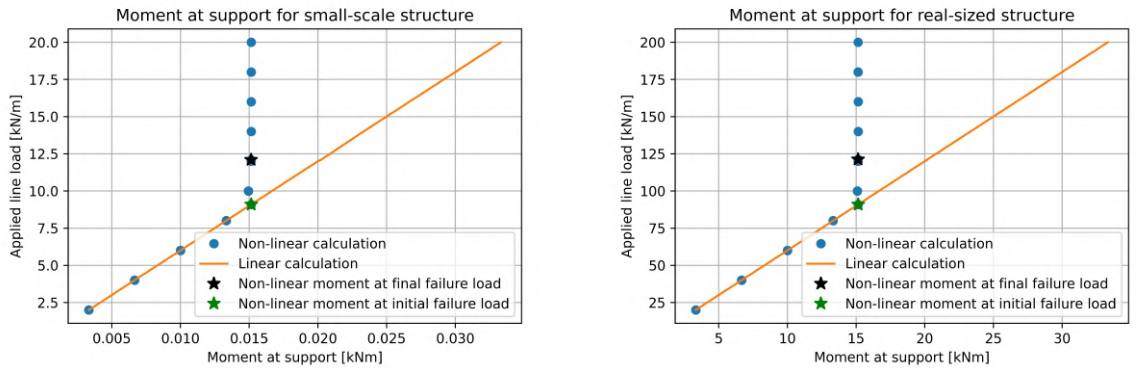

(a) Force-Moment diagram of the small-scale beam.

(b) Force-Moment diagram of the real-sized beam.

Figure 5.8: Force-Moment diagram for the nodal moment of both the small-scale beam 5.8a and the real-sized beam 5.8b. Both the linear and non-linear calculations are depicted.

The nodal moment becomes constant when the plastic moment capacity of the hinges is reached. It cannot take any more loading and the fixed supports become hinges. This is depicted in Figure 5.8. The linear calculation stays linear infinitely. The conversion rules do apply here too. The moments in the small-scale structure are one-hundredth of the real-sized structure for both the linear and non-linear calculations. Furthermore, it is known that for this system the nodal moments have a magnitude twice

as large as the moments at midspan. This is true for the linear calculation and partially true for the non-linear calculation. Figure 5.9 illustrates the relation between the absolute value of the nodal moment and the moment at midspan for both structures.

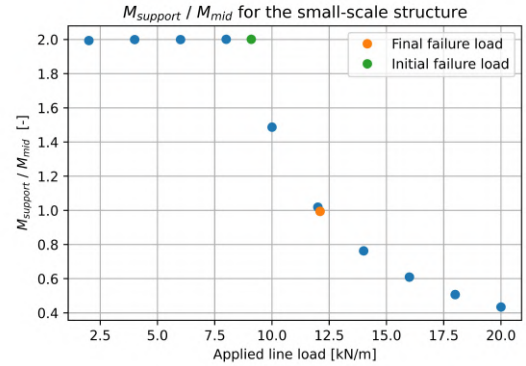

(a) Relation between $M_{support}$ and M_{mid} for the small-scale beam.

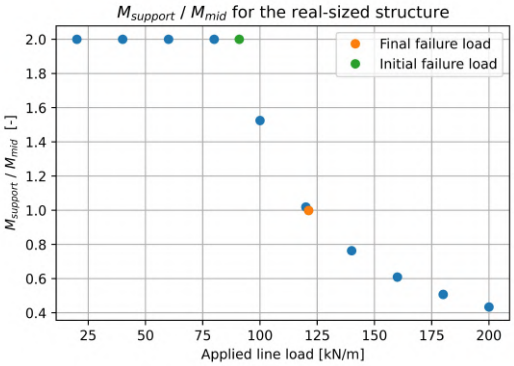

(b) Relation between $M_{support}$ and M_{mid} for the real-sized beam.

Figure 5.9: Relation between $M_{support}$ and M_{mid} for both structures when subjected to the physical non-linear calculation. The initial factor is 2, but this changes as the applied load increases.

The relation between the nodal moment and the moment at midspan follows general structural mechanics for the first four loads which range from 2 kN/m to 8 kN/m and 20 kN/m to 80 kN/m. The moment at midspan keeps increasing after this point, but the nodal moment stays constant. This can also be derived from Figures 5.7 and 5.8 where the first four points show linear behaviour in the non-linear calculation.

The line load is plotted against the deformation to see the development of the failure mechanism. the structure has failed when the displacements go to infinity. Figure 5.10 illustrates these diagrams.

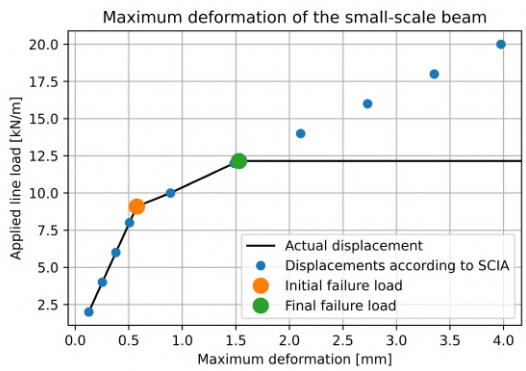

(a) Force-displacement diagram of the small-scale beam

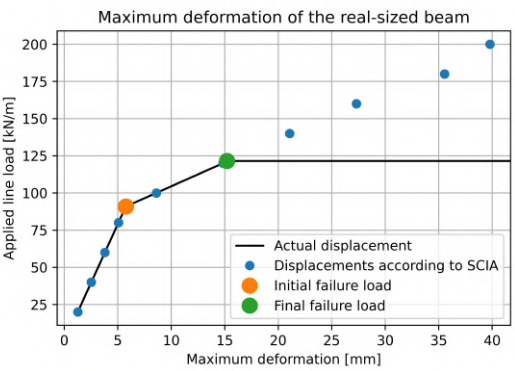

(b) Force-displacement diagram of the real-sized beam

Figure 5.10: Force displacement diagram for the statically indeterminate beams. The structure fails when the final final failure load is reached

SCIA Engineer does not allow plastic behaviour of 1D beams. The displacement therefore increases even after the final failure load is reached. However, the structure becomes a mechanism when the final failure load is reached. This is shown with the black lines in Figure 5.10. At the initial failure load, the two fixed supports become hinges and the structure is still kinematically determined.

Non-linear moment diagrams for both the small-scale structure and the real-sized structure for the failure load are depicted in Figure 5.11. The nodal moments and the moment at midspan are only identical in this instance.

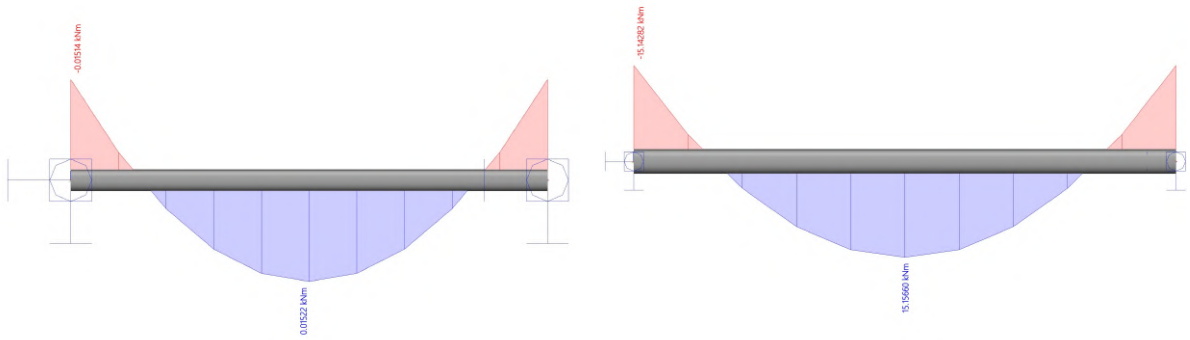

(a) Moment diagram of the small-scale beam

(b) Moment diagram of the real-sized beam

Figure 5.11: Moment diagram of the small-scale and real-sized statically indeterminate beams when subjected to their failure load. These were retrieved from SCIA Engineer.

In conclusion, the statically indeterminate beam follows the conversion rules. All moments in the small-scale structure are one-hundredth of the real-sized structure and the applied loads on the small-scale structure were one-tenth of the real-sized structure.

6

Analysis of a steel Vierendeel girder

The steel Vierendeel girder (Pons-Poblet, 2019) is similar to the steel truss. However, a Vierendeel girder does not have inclined members. Unlike the steel truss, the Vierendeel girder has rigid connections and fixed supports. Node N7 can still move horizontally, but it cannot rotate. Furthermore, the other geometrical properties are similar to the truss. The real-sized girder is 6 m long and 1 m tall and the small-scaled girder is 0.6 m long and 0.1 m tall. Finally, the steel strength is S355. Figure 6.1 illustrates this Vierendeel girder with all its node and member labels.

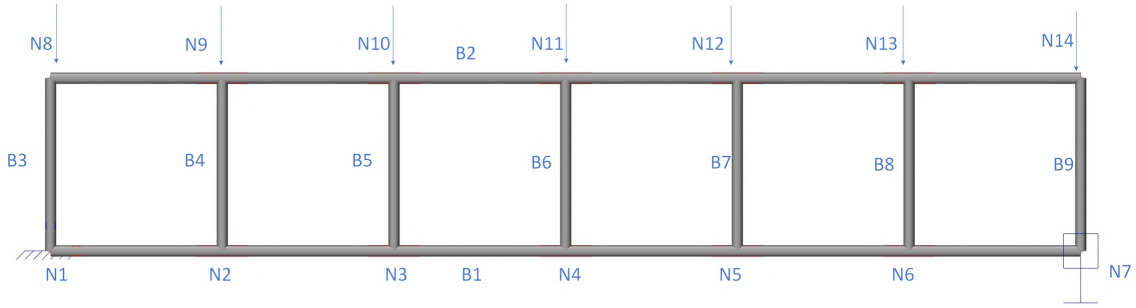

Figure 6.1: SCIA Engineer model of the Vierendeel girder.

The small-scale and real-sized structures will be tested on linearity and geometrical non-linearity. The focus will be on node N8 because this node will have large horizontal deformations due to the buckling shape of the structure.

6.1. Moments and displacements with a linear calculation

This Vierendeel girder is prone to buckling. Therefore, a linear stability calculation was done in SCIA Engineer, with an applied load of 1 kN on all upper nodes of the small-scale structure and with an applied load of 100 kN on all upper nodes of the real-sized structure. Figures 6.2 and 6.3 illustrate the buckling shape of the first buckling mode of both the small-scale and real-sized Vierdendeel girder respectively.

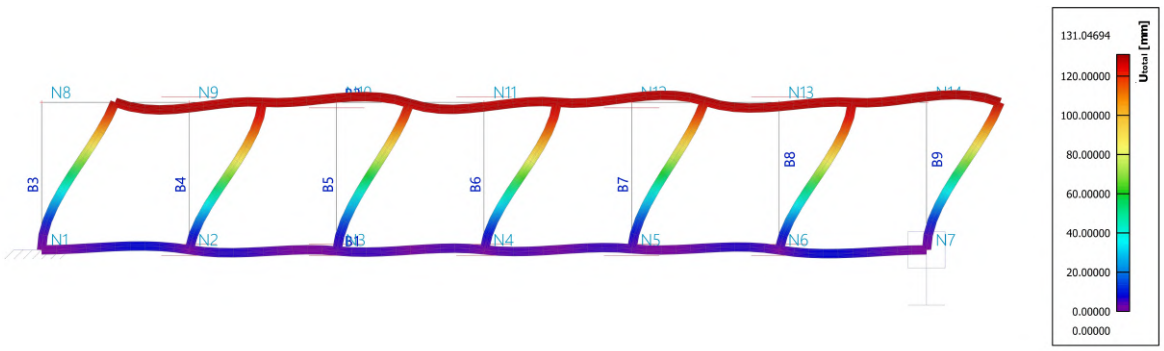

Figure 6.2: Linear stability analysis of the small-scale structure. 7 point loads of 1 kN each were applied on the upper nodes.

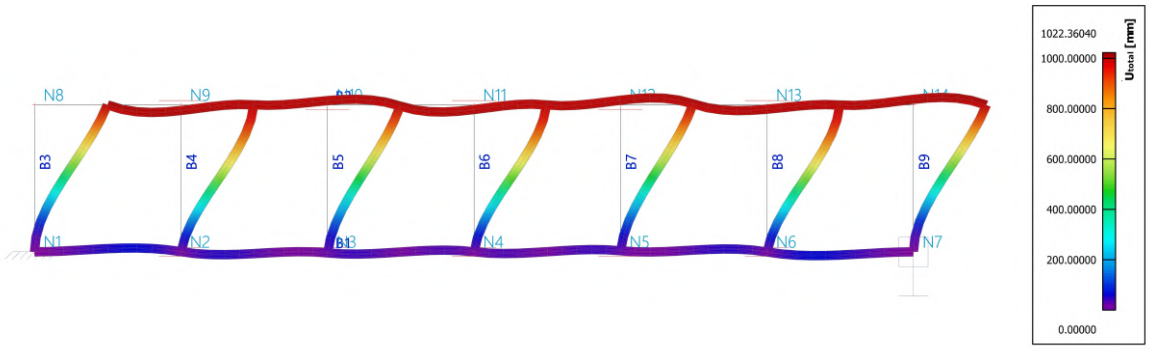

Figure 6.3: Linear stability analysis of the real-sized Vierendeel girder. 7 point loads of 1 kN each were applied on the upper nodes.

The buckling factor of the small-scale Vierendeel girder is 11.58 and it is 11.59 for the real-sized structure. The difference is negligible. The critical beam will buckle when the normal force in the critical beam is around 11.6 times higher than it is in the stability analysis. Therefore, the tested loads range from 1 kN to 9 kN for the small-scale structure and 100 kN to 900 kN for the real-sized structure. Forces larger than these give errors. Node N8 has large horizontal deformation because the structure is unbraced. Figure 6.4 illustrates the displacement of node N8 computed with a linear calculation for both the small-scale and real-sized Vierendeel girder.

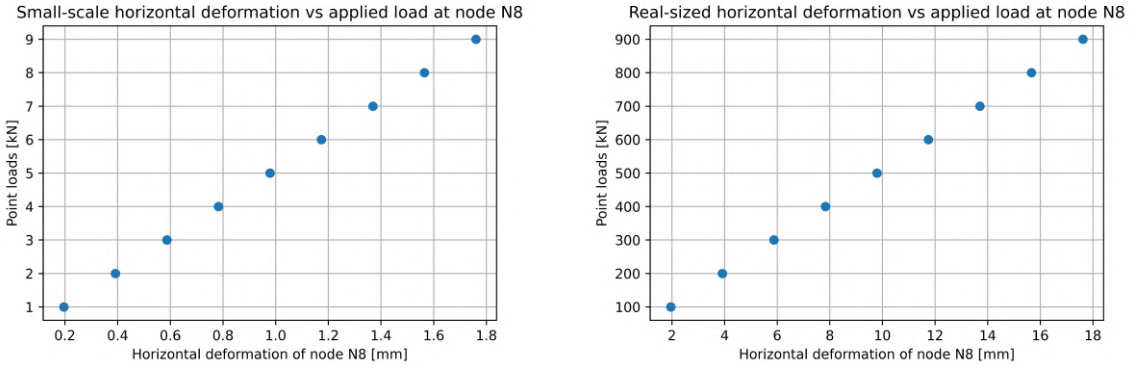

(a) Applied load vs linear deformation of node N8 of the small-scale Vierendeel girder.

(b) Applied load vs linear deformation of node N8 of the real-sized Vierendeel girder.

Figure 6.4: Linear displacement of node N8 of both the small-scale and real-sized Vierendeel girders. The applied point loads range from 1 kN to 9 kN and 100 kN to 900 kN.

Figures 6.5 and 6.6 visualize the small-scale and real-sized displacements of the entire structures. The applied load in these cases was 9 kN and 900 kN.

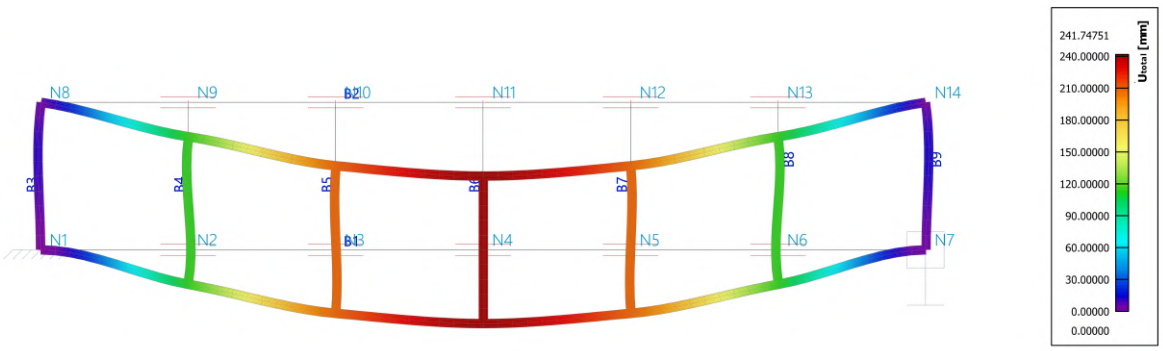

Figure 6.5: Linear deformation of the small-scale deformation when subjected to point loads of 9 kN on the upper nodes.

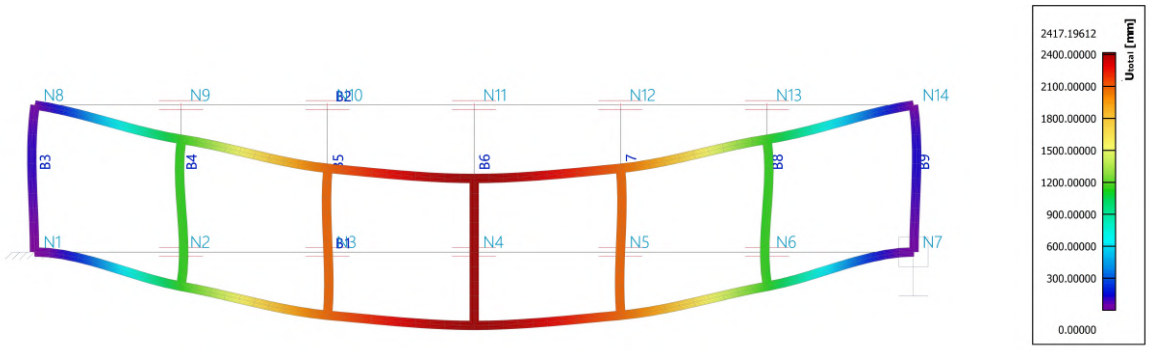

Figure 6.6: Linear deformation of the real-sized deformation when subjected to point loads of 900 kN on the upper nodes.

The small-scale displacements are a factor of 10 smaller than the real-sized. displacements. The conversion rules do apply to a linear material behaviour calculation. The moments in node N8 are computed in addition to the horizontal displacement. Figure 6.7 illustrates these diagrams.

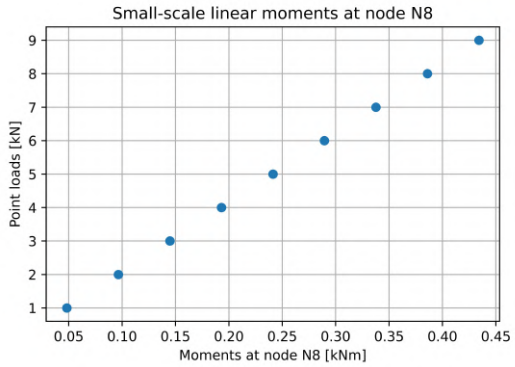

(a) Applied load vs linear moment of node N8 of the small-scale Vierendeel girder.

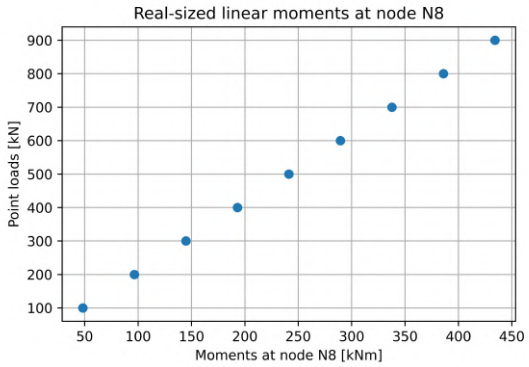

(b) Applied load vs linear moment of node N8 of the real-sized Vierendeel girder.

Figure 6.7: Linear moment of node N8 of both the small-scale and real-sized Vierendeel girders. The applied point loads range from 1 kN to 9 kN and 100 kN to 900 kN.

The moments also follow the conversion rules. The moments in the real-sized structure are 100 times larger than the small-scale structure.

6.2. Moments and displacements with a non-linear calculation

For the geometrical non-linear analysis, both structures had initial buckling imperfections of 1 mm for the small-scale structure and 10 mm for the real-sized structure. In comparison to the linear calculation, the horizontal deformation of node N8 is computed with a geometrical non-linear calculation. Figure 6.8 illustrates the deformation of node N8 vs the applied point loads. The deformation computed with the linear calculation is also illustrated in Figure 6.8.

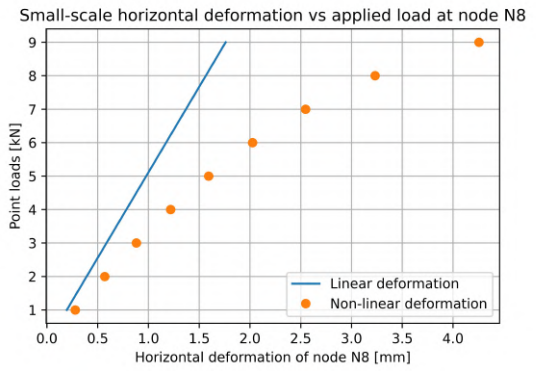

(a) Applied load vs non-linear deformation of node N8 of the small-scale Vierendeel girder.

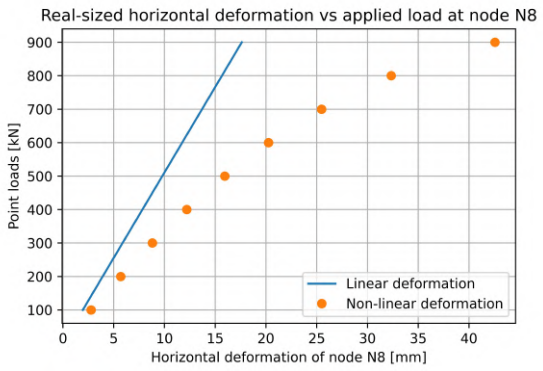

(b) Applied load vs non-linear deformation of node N8 of the real-sized Vierendeel girder.

Figure 6.8: Non-linear displacement of node N8 of both the small-scale and real-sized Vierendeel girders. The applied point loads range from 1 kN to 9 kN and 100 kN to 900 kN.

The non-linear deformations are significantly larger than the linear deformations. Furthermore, the non-linear horizontal displacements in the small-scale Vierendeel girder are 10 times smaller than in the real-sized Vierendeel girder, which means that the conversion rules apply. For visualisation purposes, the non-linear deformations of both Vierendeel girders when subjected to point loads of 9 kN and 900 kN are illustrated in Figures 6.9 and 6.10.

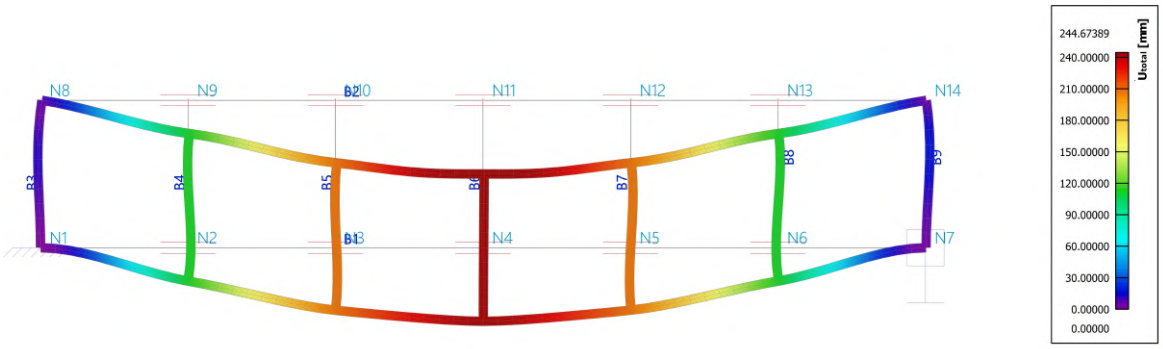

Figure 6.9: Non-linear deformation of the small-scale deformation when subjected to point loads of 9 kN on the upper nodes.

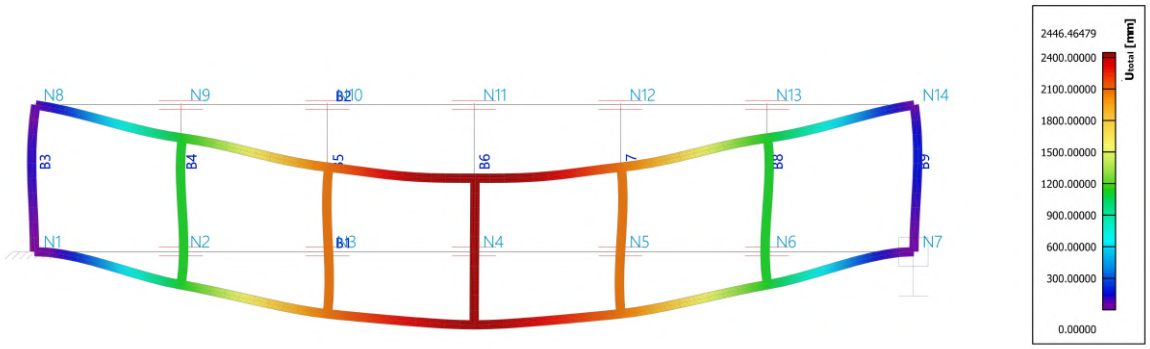

Figure 6.10: Non-linear deformation of the real-sized deformation when subjected to point loads of 900 kN on the upper nodes.

The maximum deformation in the small-scale Vierendeel girder is 244.67 mm and the real-sized Vierendeel girder's maximum deformation is 2446.47 mm, which is 10 times larger than the small-scale maximum deformation. This reaffirms the conversion rules. Finally, the moments computed with a non-linear calculation are illustrated in Figure 6.11.

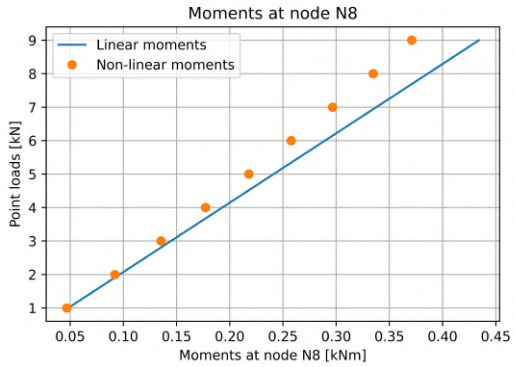

(a) Applied load vs non-linear moment of node N8 of the small-scale Vierendeel girder.

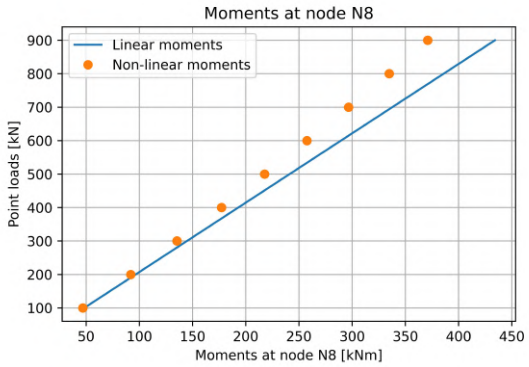

(b) Applied load vs non-linear moment of node N8 of the real-sized Vierendeel girder.

Figure 6.11: Non-linear moment of node N8 of both the small-scale and real-sized Vierendeel girders. The applied point loads range from 1 kN to 9 kN and 100 kN to 900 kN.

The non-linear moments are slightly larger than the linear moments. Furthermore, the moments at node N8 in the real-sized Vierendeel girder are 100 times larger than the moments in the small-scale Vierendeel girder, which is in line with the conversion rules.

7

Analysis of a Concrete Two-way Slab

A concrete two-way slab is one in which the forces are transferred in two directions. Therefore, a rectangular two-way slab has four rigid line supports (Lukovic, 2023). Two rectangular slabs are modelled in SCIA Engineer. The small-scale slab has a length of 1 m and its width is 0.5 m. Its thickness is 10 mm and it is supported on its four sides with rigid line supports in which one of the rigid line supports is hinged. Otherwise, the structure would be kinematically indeterminate. The dimensions of the real-sized two-way slab are a factor of 10 larger than the small-scale slab. Figure 7.1 illustrates this two-way slab.

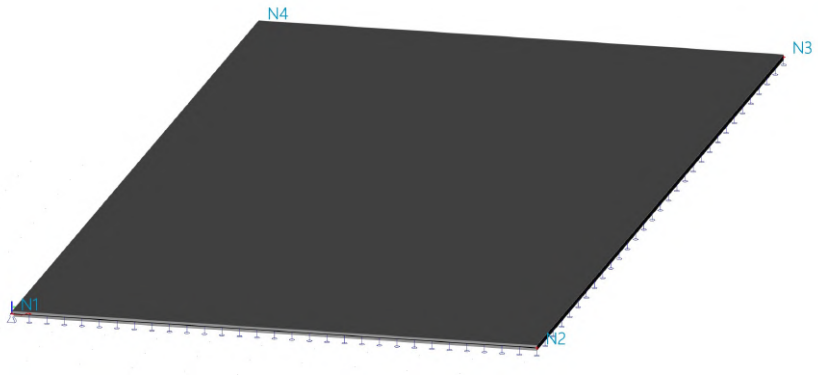

Figure 7.1: SCIA Engineer model of the concrete two-way slab.

This chapter is divided into two parts. First, the structure will be analysed on its linear material behaviour. Second, it will be analysed on its geometrical non-linear material behaviour. The material behaviour of concrete is changed in SCIA Engineer to elastic following the Von-Mises criterion (Kavoura et al., 2022) to obtain large displacements in the structure. The structure is subjected to a distributed load in the z-direction. Therefore, it is not prone to buckling. To achieve buckling a member should be loaded in compression and not in bending. Finally, the chosen concrete strength class is C30/37, which means that the compressive strength of this type of concrete ranges between 30 MPa and 37 MPa. 30 stands for its compressive strength tested on a cylindrical block and 37 is tested on a cubic block (Pancar, 2016).

7.1. 3D stresses and displacements with a linear calculation

This section delves into the linear response of the structure, testing both the stresses and displacements in the middle of this two-way slab. Both structures are subjected to loads ranging from 1 kN/m^2 to 14 kN/m^2. Figure 7.2 shows the 3D stresses against the distributed load for both structures. The stress distribution is linear and equals zero in the middle of the cross-section. There is a compressive stress in the top fibre and a tensile stress in the bottom fibre of the slab. The absolute values of these stresses are identical. Therefore only the maximum (positive) tensile stress is plotted.

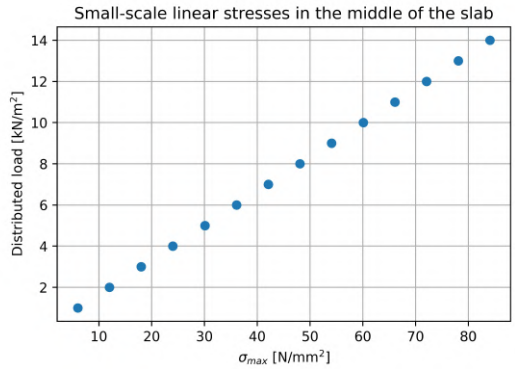

(a) Distributed load vs 3D linear stresses in the small-scale structure.

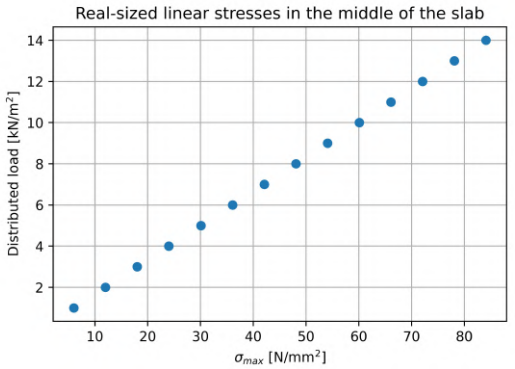

(b) Distributed load vs 3D linear stresses in the real-sized structure.

Figure 7.2: A plot of the distributed load vs the 3D stresses in both the small-scale and real-sized concrete two-way slab.

The stresses in both structures are identical, which is in line with the conversion rules. The same can be said for the displacement in the middle of the slab computed with a linear calculation. Figure 7.3 shows these displacements vs an increasing distributed load.

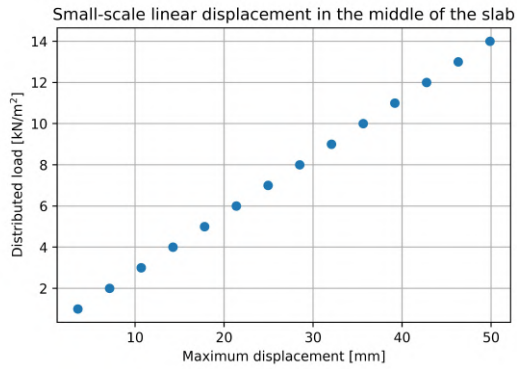

(a) Distributed load vs linear displacements in the small-scale structure.

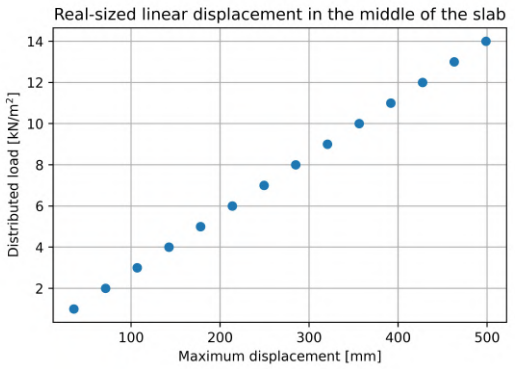

(b) Distributed load vs linear displacements in the real-sized structure.

Figure 7.3: A plot of the distributed load vs the displacements in the middle of both the small-scale and real-sized concrete two-way slab.

Figures 7.4 and 7.5 show the displacement of the structures when subjected to a load of 14 kN/m^2. The displacements in the real-sized structure are 10 times larger than the small-scale structure.

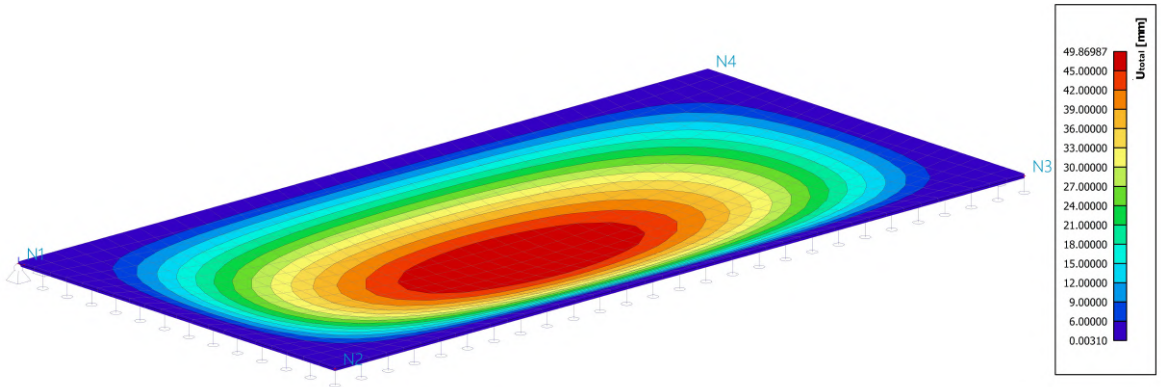

Figure 7.4: Linear displacement of the small-scale two-way slab when subjected to a distributed load of 14 kN/m^2.

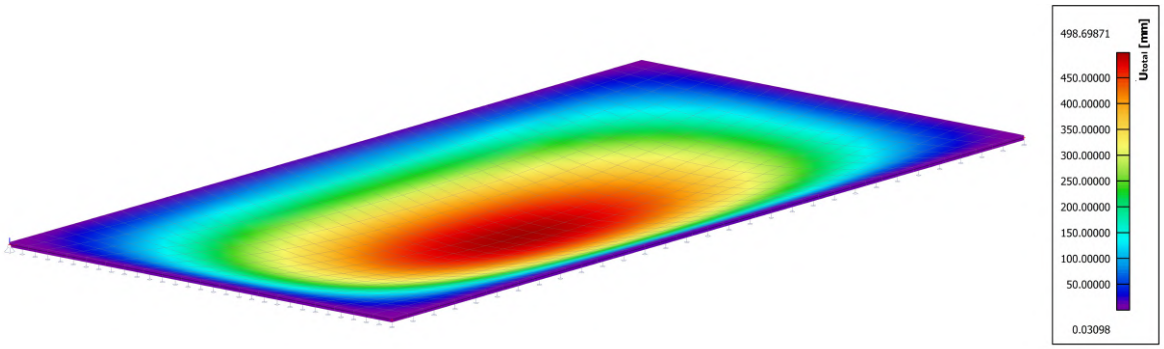

Figure 7.5: Linear displacement of the real-sized two-way slab when subjected to a distributed load of 14 kN/m^2.

The maximum displacement in the small-scale two-way slab is 49.87 mm and this displacement is 498.7 mm in the real-sized two-way slab. Therefore, the conversion rules do apply to linear material behaviour. The displacements in the real-sized two-way slab are 10 times larger than in the small-scale two-way slab and the stresses are identical in both slabs.

7.2. 3D stresses and displacements with a non-linear calculation

The material behaviour of the concrete slab is changed to elastoplastic to obtain large displacements in the non-linear calculation. The stresses should change when the compressive strength of concrete is reached. The 3D non-linear maximum stresses are plotted for both structures when subjected to loads ranging from 1 kN/m^2 to 14 kN/m^2. Figure 7.6 illustrates this for both the small-scale and real-sized slab.

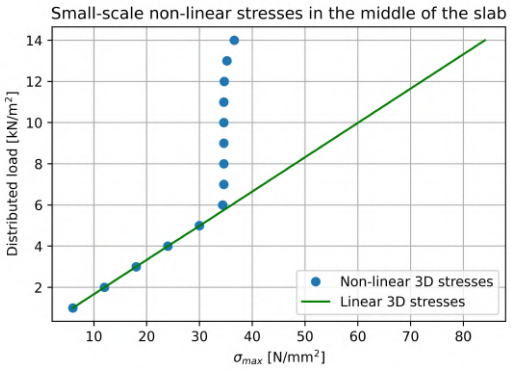

(a) Distributed load vs non-linear 3D stresses in the small-scale structure.

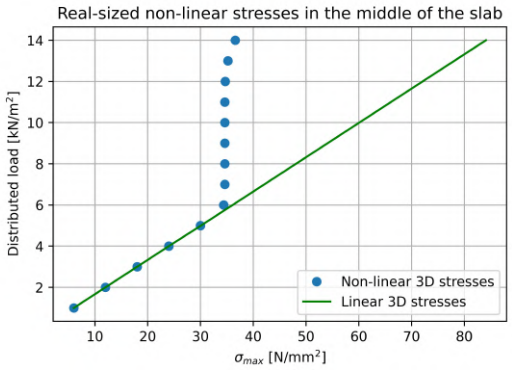

(b) Distributed load vs non-linear 3D stresses in the real-sized structure.

Figure 7.6: A plot of the distributed load vs the non-linear 3D stresses in both the small-scale and real-sized concrete two-way slab.

The stresses do not increase for a while when 35 MPa is reached. However, after exceeding 35 MPa, the stresses become too large and the structure fails. A load of 15 kN/m^2 failed both slabs. However, both structures acted similarly. The stresses do not differ. therefore, the stress conversion rule applies. Similarly, the non-linear maximum displacements are plotted for both structures. Figure 7.7 depicts these displacements for both structures.

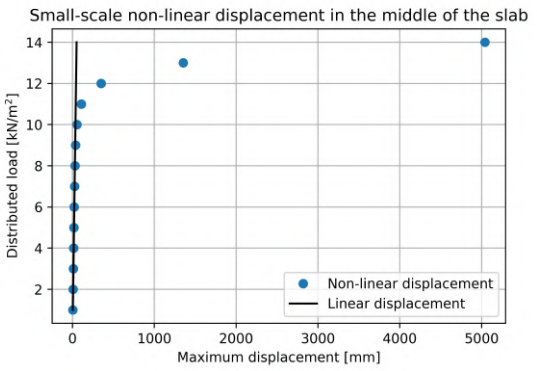

(a) Distributed load vs non-linear displacements in the small-scale structure.

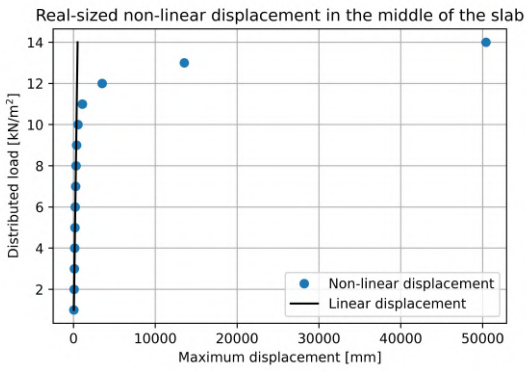

(b) Distributed load vs non-linear displacements in the real-sized structure.

Figure 7.7: A plot of the distributed load vs non-linear displacements in the middle of both the small-scale and real-sized concrete two-way slab.

There are significant differences between the displacements computed with a linear calculation and the displacements computed with a non-linear calculation. The difference becomes significant when the structures are subjected to a load of 12 kN/m^2. Furthermore, the conversion rules for displacements apply because the displacements in the real-sized structure are 10 times larger than the small-scale structure. Figures 7.8 and 7.9 show the non-linear displacements of both structures outputted by SCIA Engineer when subjected to a load of 14 kN/m^2. The displacements in Figures 7.4 and 7.5 are relatively small compared to the displacements in Figures 7.8 and 7.9. This difference reaffirms the presence of non-linearity.

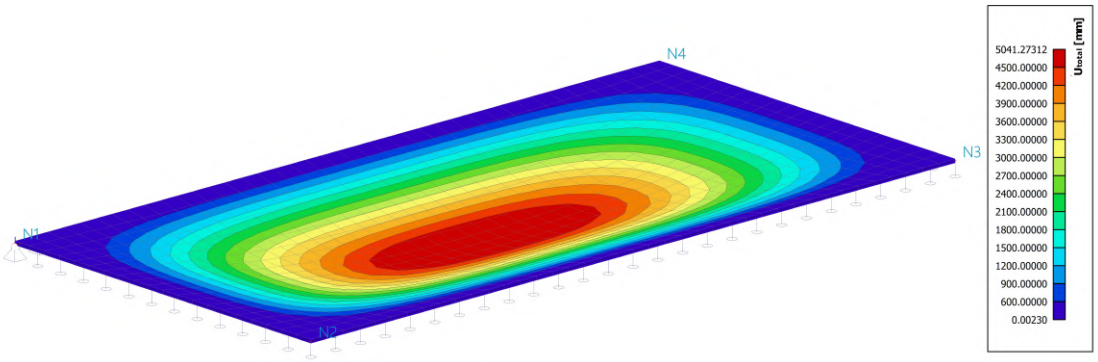

Figure 7.8: Non-linear displacement of the small-scale two-way slab when subjected to a distributed load of 14 kN/m^2.

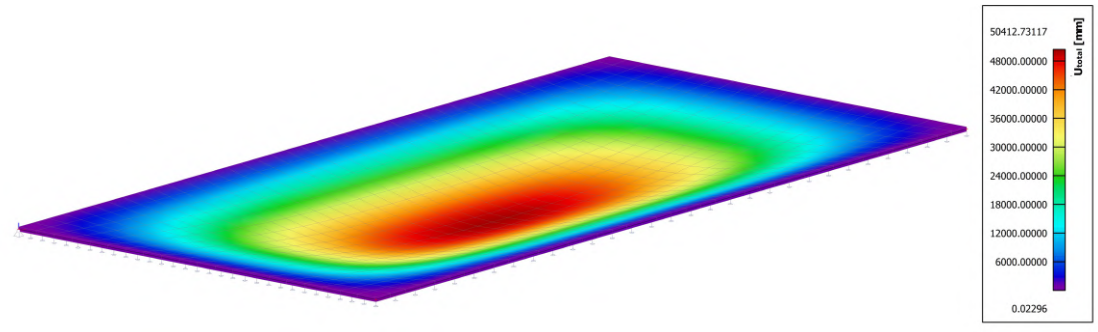

Figure 7.9: Non-linear displacement of the real-sized two-way slab when subjected to a distributed load of 14 kN/m^2.

In conclusion, the concrete two-way slab does follow the conversion rules from small-scale structures to real-sized structures, even when changing the material behaviour to elastoplastic.

8

Analysis of a Concrete Shell Roof

Shell roofs are civil engineering structures with an efficient design (Ramm, 2004). Therefore, two shell roofs are modelled in SCIA Engineer. The geometrical properties of both structures are chosen. The thicknesses are 20 mm and 200 mm. They cover a squared area of 10 m by 10 m and 1 m by 1 m. The heights of node N5 are 5 m and 0.5 m and node N6 are 2.5 and 0.25 m. The bows from N1 to N2 and N3 to N4 have radii of 5/0.5 m and 2.5/0.25 m respectively. Finally, the chosen concrete class is C30/37. Figure 8.1 shows the SCIA Engineer model of the concrete shell roof.

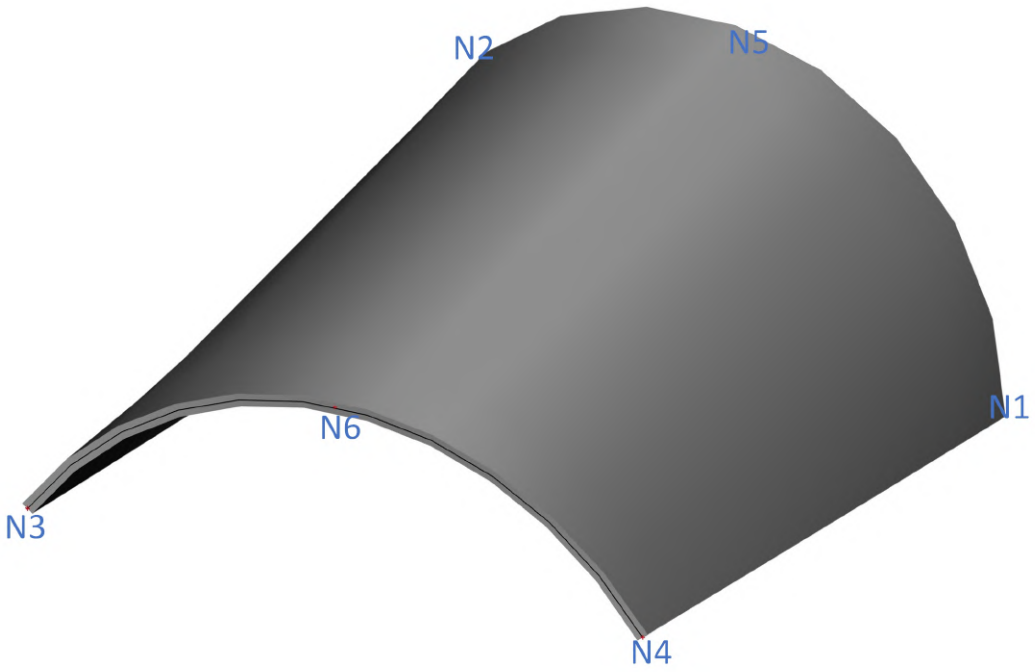

Figure 8.1: A shell roof modelled in SCIA Engineer.

8.1. 3D stresses and displacements with a linear calculation

Both structures were subjected to several distributed loads ranging from 250 to 2750 kN/m^2 with a stepsize of 250 kN/m^2. This range was chosen because the critical buckling load according to a linear calculation is 2657.1 kN/m^2. This is done by performing a linear stability analysis in SCIA Engineer with a distributed load of 5 kN/m^2. The program then outputs a load factor α of 531.42. The formula for the critical buckling force follows in Equation 8.1:

$$p_{buc} = \alpha \cdot p_{applied} = 531.42 \cdot 5 = 2657.1 kN/m^2, \tag{8.1}$$

where α is the buckling factor and $p_{applied}$ is the applied distributed load. This linear buckling analysis is done for both structures, which yields the same critical buckling force. Figure 8.2 shows this buckling mode.

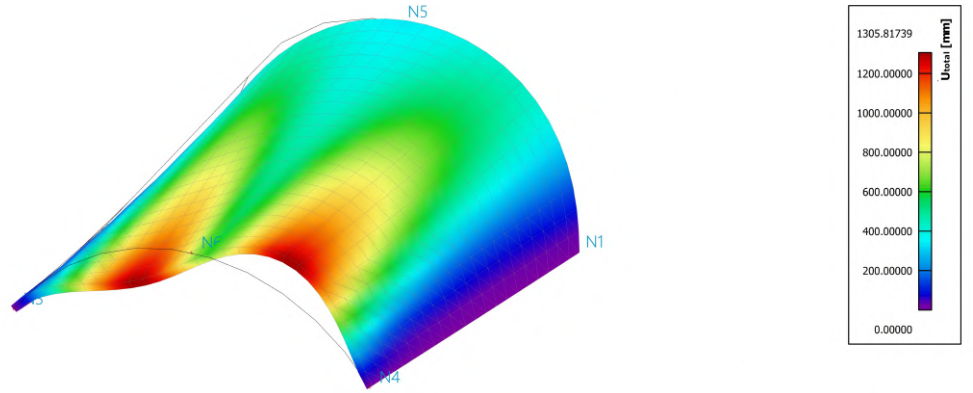

Figure 8.2: Deformation in the real-sized shell roof when performing linear stability analysis with a distributed load of 5 kN/m^2. In the upper-left part of the figure, we see the buckling factor corresponding to this distributed load which is highlighted in blue.

As Figure 8.2 shows, the bow connecting N2, N3 and N6 buckle. To analyse the behaviour in this bow, the displacements of N6 are computed with the loads ranging from 250 kN/m^2 to 2752 kN/m^2 including the buckling force of 2657.1 kN/m^2. Figure 8.3 shows the magnitude of deformation of N6 against the increasing distributed load.

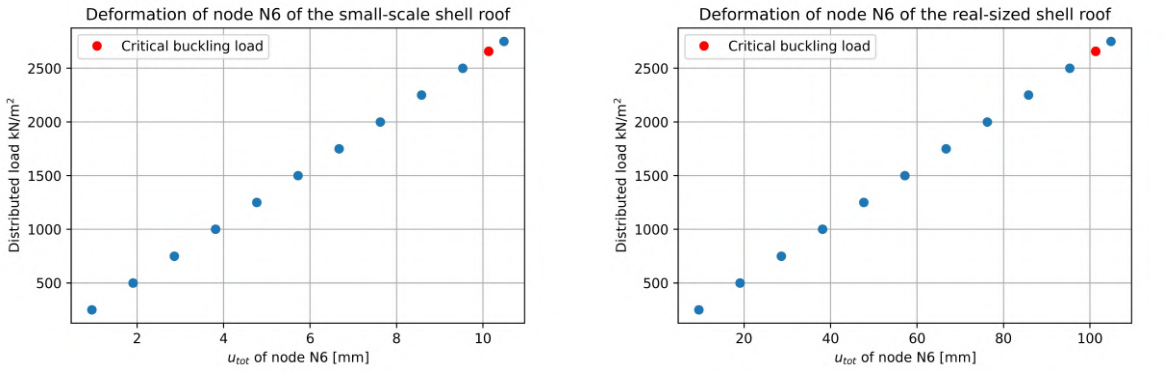

(a) Force-displacement diagram of the small-scale shell-roof. **(b)** Force-displacement diagram of the real-sized shell-roof.

Figure 8.3: Force-displacement diagrams of both the small-scale and the real-sized shell roof when computed with a linear calculation in SCIA Engineer.

As expected, the nodal displacements in the small-scale structure are exactly one-tenth of the real-sized structure. Additionally, the displacements are increasing linearly with the force, which is also expected.

Second, the stresses in both structures can be compared. The stresses are compared for an applied load of 2750 kN/m^2. Figures 8.4 and 8.5 show the 3D stresses of the small-scale and real-sized structures respectively.

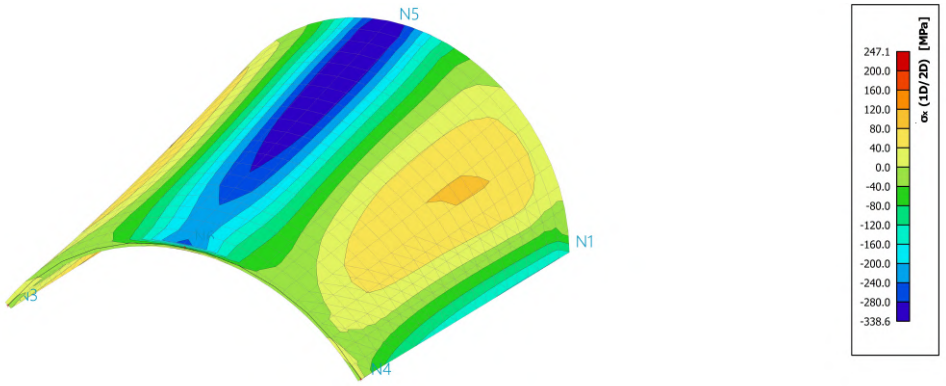

Figure 8.4: 3D stresses of the small-scale shell roof when subjected to a distributed load of 2750 kN/m^2 computed with a linear calculation.

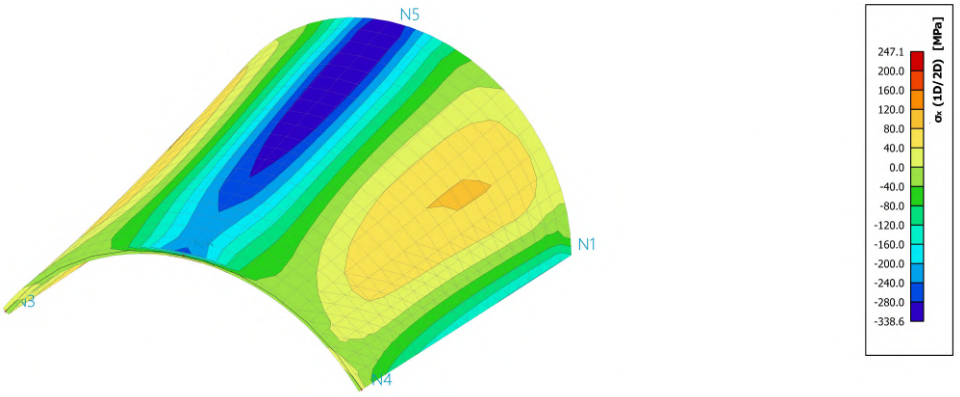

Figure 8.5: 3D stresses of the real-sized shell roof when subjected to a distributed load of 2750 kN/m^2 computed with a linear calculation.

According to the conversion rules, the stresses in the small-scale structure should be identical to the stresses in the real-sized structure. We can see this in Figures 8.4 and 8.5. The stresses range from -338.6 MPa to 247.1 MPa in both structures.

8.2. 3D stresses and displacements with a non-linear calculation

In this section, two kinds of geometrical non-linearity will be tested. First, a non-linear calculation follows with bow imperfections that follow buckling data. Second, the structure is computed with a non-linear calculation using a simple curvature as the bow imperfection.

8.2.1. Non-linearity with buckling curve imperfections

In the non-linear calculation, the shell roof has an imperfection following the buckling curve. Again, the deformation of Node N6 is computed for both the small-scale and real-sized structures. Figure 8.6 shows the non-linear and linear deformation of node N6.

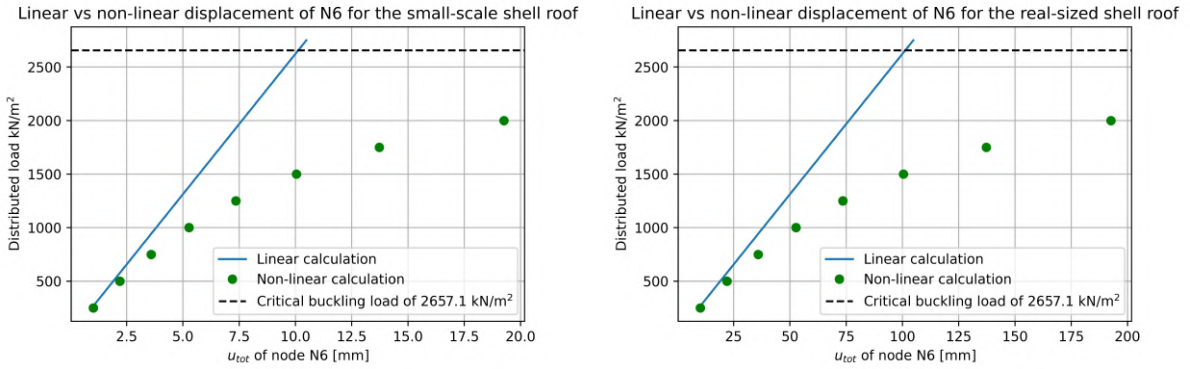

(a) Force-displacement diagram of the small-scale shell-roof. **(b)** Force-displacement diagram of the real-sized shell-roof.

Figure 8.6: Force-displacement diagrams of both the small-scale and the real-sized shell roof when computed with a non-linear calculation in SCIA Engineer.

The linear calculations were also illustrated in Figure 8.3. As we can see, the non-linear calculation yields higher displacements with a much smaller force. The buckling force, computed with the linear stability analysis cannot be reached because the structure has already become a mechanism. However, the conversion from small-scale to real-sized is accurate, as the displacements in the small-scale structure are one-tenth of the real-sized structure. Additionally, a non-linear stability calculation was done to compare the results with the linear calculation. The deformation and the load factor for a load of 5 kN/m^2 are shown in Figure 8.7. Both structures have identical buckling factors.

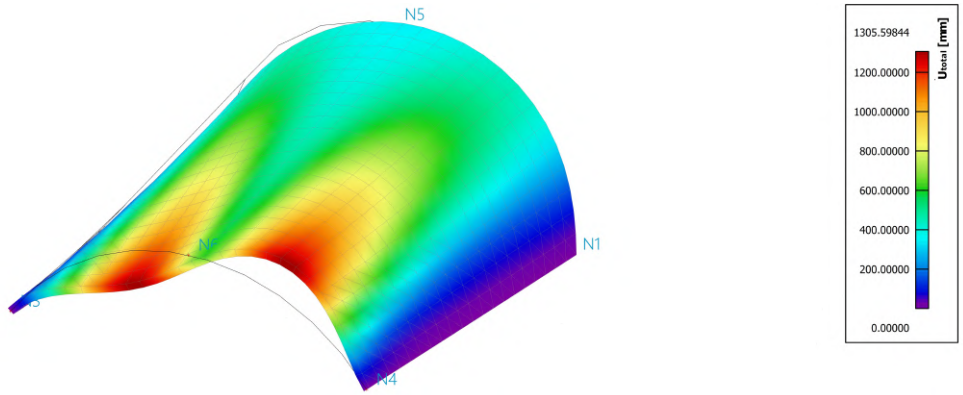

Figure 8.7: Non-linear stability calculation computed with an applied load of 5 kN/m^2 on the real-sized structure. The buckling factor is 530.66 which makes the non-linear buckling force 2653.3 kN/m^2.

The buckling factor is 530.66 which gives a critical non-linear buckling load of 2653.3 kN/m^2. The load in Figure 8.6 does not reach 2653.3 kN/m^2 for the non-linear calculation. This happens because the displacements become too large at a lower load and go to infinity. Therefore, they will never reach the buckling load.

A second important comparison is the stresses in the structures. These should be identical to be in line with the conversion rules. We do not have the results with the applied load of 2750 kN/m^2 because the structure has already become a mechanism by then. We do have the stresses for an applied load of 2000 kN/m^2. Figures 8.8 and 8.9 show the non-linear stresses for both structures for an applied load of 2000 kN/m^2.

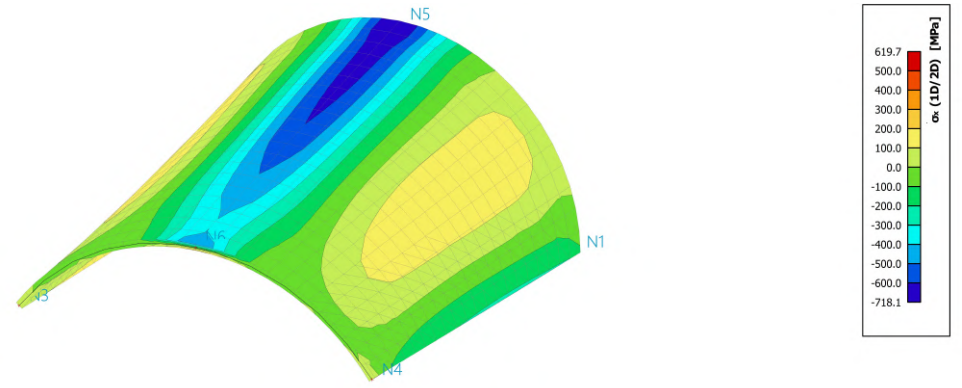

Figure 8.8: 3D stresses in the small-scale structure computed with a non-linear calculation with an applied load of 2000 kN/m^2.

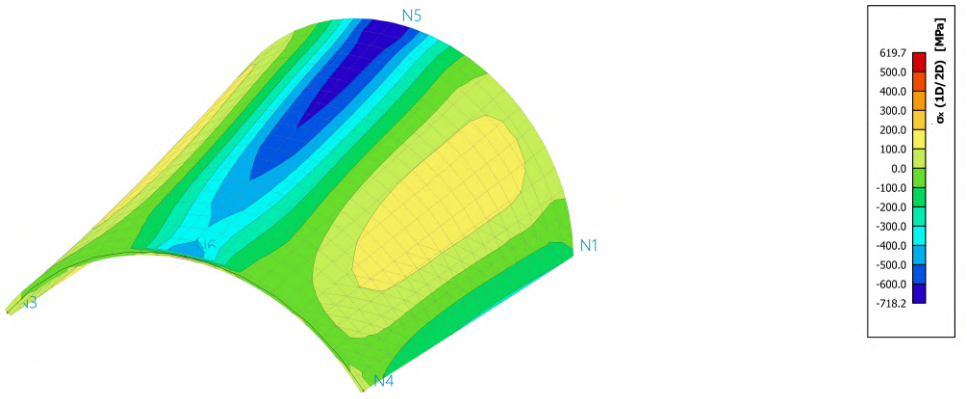

Figure 8.9: 3D stresses in the real-sized structure computed with a non-linear calculation with an applied load of 2000 kN/m^2.

The internal stresses are identical. The stresses in the small-scale structure range from -718.1 kN/m^2 to 619.7 kN/m^2 and in the real-sized structure from -718.2 kN/m^2 to 619.7 kN/m^2. The differences are small enough to be interpreted as numerical errors.

8.2.2. Non-linearity with an applied displacement following the buckling shape

In this case, a displacement of 1 mm and 10 mm was applied to the structures. This buckling shape of the first buckling mode is integrated into this applied displacement. Similar to Figure 8.6, the displacements of node N6 computed with this non-linear calculation are illustrated in Figure 8.10.

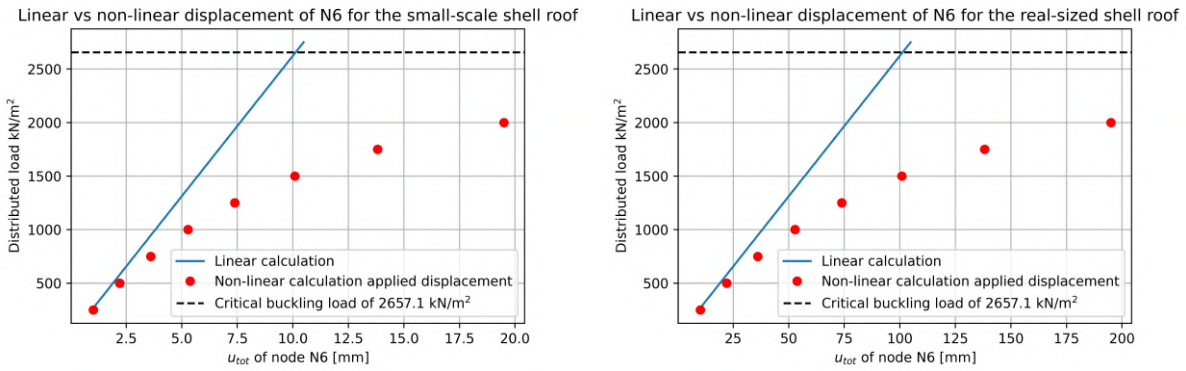

(a) Force-displacement diagram of the small-scale shell-roof.

(b) Force-displacement diagram of the real-sized shell-roof.

Figure 8.10: Force-displacement diagrams of both the small-scale and the real-sized shell roof when computed with a non-linear calculation and an applied displacement in SCIA Engineer.

The nodal displacement of N6 can be computed with the existing conversion rules. We see small differences between the non-linear calculation with an applied displacement and the non-linear calculation with a bow imperfection that follows the buckling data. However, the non-linear calculation with this applied displacement also follows the conversion rules. We can confirm this by showing the stresses for both structures when subjected to a distributed load of 2000 kN/m^2. Figures 8.11 and 8.12 show these stresses for the small-scale and real-sized structures respectively.

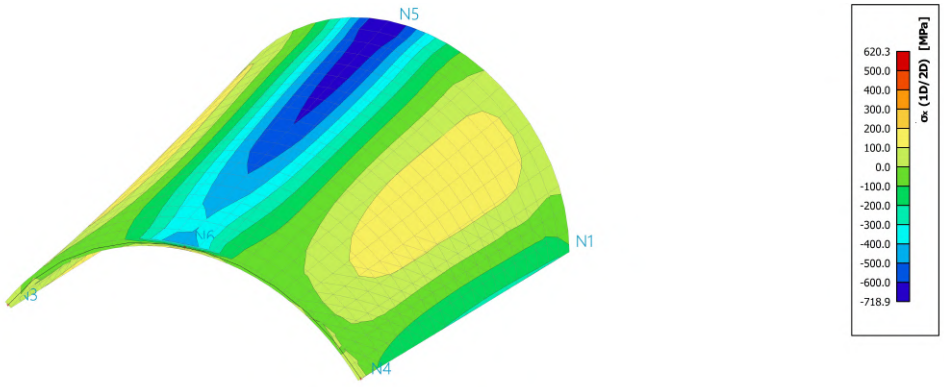

Figure 8.11: 3D stresses in the small-scale structure computed with a non-linear calculation with an applied load of 2000 kN/m^2. The nonlinearity comes from an applied displacement following the buckling shape.

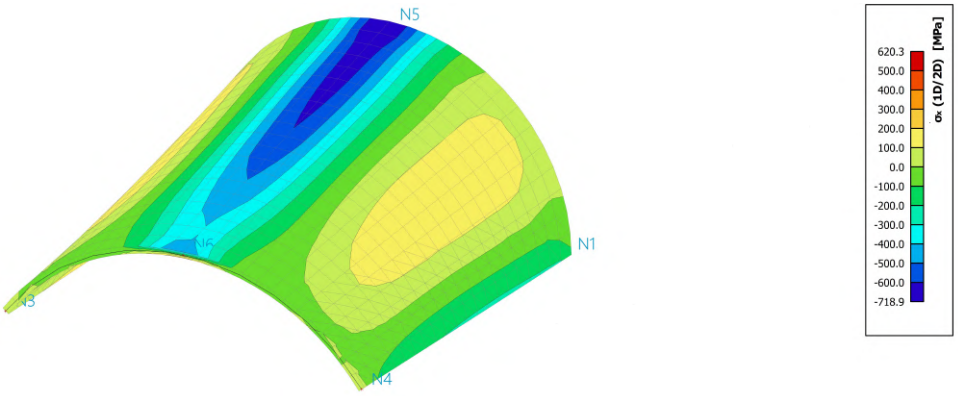

Figure 8.12: 3D stresses in the real-sized structure computed with a non-linear calculation with an applied load of 2000 kN/m^2. The nonlinearity comes from an applied displacement following the buckling shape.

The 3D non-linear stresses in the small-scale structure range from -718.9 kN/m^2 to 620.3 kN/m^2 and from -718.9 kN/m^2 to 620.3 kN/m^2. Again, the differences are small enough to be interpreted as numerical errors.

In conclusion, the conversion rules do apply to a concrete shell roof. We see that there is a significant difference between the linear and non-linear displacements. This means that we are testing non-linearity instead of linearity.

9 Conclusion

This research analysed five types of structures on linear and non-linear material behaviour. The goal was to analyse whether the conversion rules from small-scale to real-sized structures also work for physical and geometrical non-linear material behaviour.

Geometrical non-linearity

The geometrical non-linear analysis was done for the steel truss, Vierendeel girder, the statically determinate beam, and the concrete shell roof. The conversion rules for linear material behaviour worked for all structures. There were marginal errors in the conversion, but SCIA Engineer makes these numerical errors when doing an iterative calculation. Namely, geometrical non-linear calculations are iterative. All numerical values of the figures used in these analyses are listed in Appendix A.

Physical non-linearity

The physical non-linear analysis was done for the steel statically indeterminate beam and the concrete plate. However, this was done in addition to geometrical non-linearity. Both structures were subjected to large displacements which yield additional internal forces. The plate was analysed with an elasto-plastic stress-strain curve following the Von Mises yield criterion (Kavoura et al., 2022) and the statically indeterminate beam was tested with the plasticity of hinges. Again, the conversion rules for these types of non-linearity worked. There were some marginal errors, but these are negligible.

Finally, the following research question is answered: “There are conversion rules for deflection and stresses from small-scale structures to real-sized structures. Do these apply to non-linear behaviour too?” After extensive analysis of multiple different structures, it can be concluded that the conversion rules from the studied small-scale to real-sized structures also apply to physical and geometrical non-linear material behaviour.

Future work

This research only looked at structures with symmetrical and homogeneous cross-sections. Namely, circular steel cross-sections for the trusses and beams and rectangular cross-sections for the concrete two-way slab and shell roof. However, composite or asymmetrical cross-sections have not been researched. Asymmetrical cross-sections yield forces in both x- and y-direction, even when they are loaded in one direction. Composite cross-sections are prone to slipping at the intersection between the two materials. For future work, structures with asymmetrical and composite cross-sections can be analysed.

References

Ahmadpour, s. m., Fariba, F., & h.bahrami. (2017, March). *A new method for the correction of stress–strain curves after bulging in metals*.

Alsayed, A. (2021). Physics of open fractures: Reconsidering tissue viability, contamination risk and importance of wound debridement. *Journal of Applied Mathematics and Physics*, *09*, 176–182. https://doi.org/10.4236/jamp.2021.91012

Cantor, B. (2020, July). 207Hooke's Law: Elasticity. In *The Equations of Materials*. Oxford University Press.

Chan, S. (2001). Non-linear behavior and design of steel structures. *Journal of Constructional Steel Research*, *57*(12), 1217–1231. https://doi.org/https://doi.org/10.1016/S0143-974X(01)00050-5

Çopuroğlu, O. (2018). *Mechanical properties of materials*.

Davis, J. R. (2004). *Tensile testing*. ASM international.

Hartsuijker, C. (2013, January 1). *Mechanica: Statisch onbepaalde constructies en bezwijkanalyse*.

Hoogenboom, P. (2023, November 16). *Notes on shell structures*. https://phoogenboom.nl/B&B_schaal_scaling_rules.pdf

Hoogenboom, P. C. J. (n.d.). *Course ct3280 shell roofs*. https://phoogenboom.nl/B&B_schaal_0.html

Kavoura, F., de Vries, P., & Steel and Composite Structures. (2022, February 12). *Beton staalconstructies*.

Lukovic, M. (2023, March). *Challenge the future* (tech. rep.).

Machacek, J., & Cudejko, M. (2011). Composite steel and concrete bridge trusses. *Engineering Structures*, *33*(12), 3136–3142. https://doi.org/https://doi.org/10.1016/j.engstruct.2011.08.017

Mishra, G. (2024, April 3). *Types of structural design and its processes*. https://theconstructor.org/structural-engg/types-structural-design-process/1673/

Mukuvare, A. (2013, March 10). *Euler buckling*. University of Surrey. https://arnoldmukuvare.wordpress.com/wp-content/uploads/2013/02/euler-buckling-lab-2.pdf

Nemetschek Scia. (2014). *Advanced concept training*. https://downloads.scia.net/support/sciaengineer/manuals/14/training%20manuals/non%20linear%20and%20stability/[eng]advanced%20professional%20training%20non%20linear%20and%20stability%2014.0.pdf

Neville, A. (2001). *Aggregates for concrete*. Taylor Francis Group.

Pancar, E. B. (2016). Reducing thermal cracks and mitigating heat island by using glass bead in concrete pavement. *IOSR journal of mechanical and civil engineering*, *13*(04), 94–98. https://doi.org/10.9790/1684-1304049498

Pons-Poblet, J. M. (2019). *The vierendeel truss: Past and present of an innovative typology*. https://www.redalyc.org/journal/1936/193660402011/html/#:~:text=Abstract%3A%20In%20the%20late%2019th,known%20as%20the%20Vierendeel%20truss.

Ramm, E. (2004). Shape finding of concrete shell roofs. *Journal of the International Association for Shell and Spatial Structures*, *45*(1), 29–39. https://www.ingentaconnect.com/content/iass/jiass/2004/00000045/00000001/art00005

Roylance, D. (2001, January). *Finite element analysis*. Department of Materials Science; Engineering Massachusetts Institute of Technology. https://resources.saylor.org/wwwresources/archived/site/wp-content/uploads/2012/09/ME1023.2.3.pdf

Sabat, L., & Kundu, C. K. (2020). History of finite element method: A review. *Lecture notes in civil engineering*, 395–404. https://doi.org/10.1007/978-981-15-4577-1_32

Saliklis, E. (2020). Trusses. In *Structures: A studio approach* (pp. 143–158). Springer International Publishing. https://doi.org/10.1007/978-3-030-33153-5_6

SCIA. (2024). *Scia engineer* (comp. software; Version 24.0). https://www.scia.net/en/scia-engineer

Welleman, J. W. (n.d.). *Stabiliteit van het evenwicht knik en de voorschriften*. https://www.joostdevree.nl/bouwkunde2/jpgk/knik_12_knik_en_voorschriften_eurocode3_ir_j_w_welleman.pdf

Welleman, J. (n.d.). *Vergeet-mij-nietjes*. https://icozct.tudelft.nl/TUD_CT/CT3109/collegestof/invloedslijnen/files/VGN.pdf

Zavatsky, A. (n.d.). *P4 stress and strain* (tech. rep.). https://users.ox.ac.uk/~kneabz/Stress3_mt07.pdf

A

Numerical values of the plotted figures

This appendix shows all numerical values used in the plots in this report. A brief explanation is added when needed.

A.1. Numerical values of plots of the steel truss

Tables A.1 and A.2 depict the moments in the steel truss with bending stiffness.

Table A.1: Numerical data of the linear and non-linear displacements of member B10 of the small-scale steel truss with bending stiffness of Figures 4.4 and 4.8.

Load [kN]	Linear u_{tot} B10 [mm]	Non-linear u_{tot} B10 [mm]
1	0.23403	0.29099
2	0.46802	0.60586
3	0.70199	0.95863
4	0.93592	1.37648
5	1.16982	1.91904
6	1.4037	2.74166
7	1.63754	4.37779
8	1.87135	9.86328

Table A.2: Numerical data of the linear and non-linear displacements of member B10 of the real-sized steel truss with bending stiffness of Figures 4.4 and 4.8.

Load [kN]	Linear u_{tot} B10 [mm]	Non-linear u_{tot} B10 [mm]
100	2.343	2.91271
200	4.68569	6.06402
300	7.02807	9.59299
400	9.37014	13.7696
500	11.71191	19.184
600	14.05337	27.36856
700	16.39452	43.56216
800	18.73536	98.52176

Tables A.3 and A.4 depict the numerical data of the plots of the linear and non-linear moments of node N4 of the truss with bending stiffness.

Table A.3: Numerical data of linear and non-linear moments of node N4 of the small-scale truss with bending stiffness. The plots are in Figures 4.7 and 4.11.

Load [kN]	Linear moment N4 [kNm]	Non-linear moment N4 [kNm]
1	0.00038	0.00042
2	0.00076	0.00097
3	0.00115	0.00164
4	0.00153	0.00244
5	0.00191	0.00337
6	0.00229	0.00444
7	0.00268	0.00565
8	0.00306	0.00705

Table A.4: Numerical data of linear and non-linear moments of node N4 of the real-sized truss with bending stiffness. The plots are in Figures 4.7 and 4.11.

Load [kN]	Linear moment N4 [kNm]	Non-linear moment N4 [kNm]
100	0.38276	0.42288
200	0.76552	0.96917
300	1.14827	1.64125
400	1.53103	2.44165
500	1.91379	3.3735
600	2.29655	4.44157
700	2.6793	5.6561
800	3.06206	7.05471

Tables A.5 and A.6 depict the numerical data of the linear and non-linear moments of member B10 of the steel truss without bending stiffness.

Table A.5: Numerical data of normal forces of the small-scale truss without bending stiffness. The plots are in Figures 4.16 and 4.20.

Load [kN]	Linear normal force B10 [kN]	Non-linear normal force B10 [kN]
10	-35.35534	-35.0462
20	-70.71068	-69.31846
30	-106.066	-102.5434
40	-141.42141	-134.64159
50	-176.7767	-165.2098
60	-212.132	-194.5758
70	-247.48741	-222.19491
80	-282.84269	-248.2765
90	-318.19809	-272.93731
100	-353.55341	-296.38731
110	-388.90869	-318.93059
120	-424.26409	-340.96141
130	-459.61941	-347.43181
140	-494.97481	-361.0675
150	-530.33012	-372.14719
160	-565.6855	-398.21159
170	-601.04081	-413.61469
180	-636.39612	-408.79981
190	-671.7515	-412.593
200	-707.10681	-449.94281
210	-742.46213	-469.30109

Table A.6: Numerical data of normal forces of the real-sized truss without bending stiffness. The plots are in Figures 4.16 and 4.20.

Load [kN]	Linear normal force B10 [kN]	Non-linear normal force B10 [kN]
1000	-3535.53	-3504.587
2000	-7071.07	-6931.677
3000	-10606.6	-10253.88
4000	-14142.1	-13463.25
5000	-17677.7	-16519.38
6000	-21213.2	-19455.22
7000	-24748.7	-22216.13
8000	-28284.3	-24823.2
9000	-31819.8	-27288.17
10000	-35355.3	-29632.17
11000	-38890.9	-31885.76
12000	-42426.4	-34088.528
13000	-45961.9	-34728.032
14000	-49497.5	-36088.4
15000	-53033	-37192.512
16000	-56568.6	-39806
17000	-60104.1	-41347.208
18000	-63639.6	-40850.008
19000	-67175.2	-41221.94
20000	-70710.7	-44983.58
21000	-74246.2	-46930.128

Tables A.7 and A.8 depict the linear and non-linear displacement of node N4 of the steel trusses without bending stiffness.

Table A.7: Numerical data of linear and non-linear displacement of node N4 of the small-scale steel truss without bending stiffness as is shown in Figures 4.17 and 4.21.

Load [kN]	Linear u_{tot} N4 [mm]	Non-linear disp N4 [mm]
10	7.577278	7.621662
20	15.154551	15.378309
30	22.731827	23.242449
40	30.309113	31.17923
50	37.886388	39.154665
60	45.463664	47.205119
70	53.040939	55.226931
80	60.618216	63.233921
90	68.195501	71.218395
100	75.772777	79.18302
110	83.350053	87.142101
120	90.927328	95.122383
130	98.504611	101.596891
140	106.081917	108.77118
150	113.659184	115.668644
160	121.236453	123.84603
170	128.813713	130.924207
180	136.390989	137.749514
190	143.96825	144.360457
200	151.54551	152.941294
210	159.122787	160.501159

Table A.8: Numerical data of linear and non-linear displacement of node N4 of the real-sized steel truss without bending stiffness as is shown in Figures 4.17 and 4.21.

Load [kN]	Linear u_{tot} N4 [mm]	Non-linear disp N4 [mm]
1000	75.84695	76.29191
2000	151.69389	153.98307
3000	227.54082	232.65665
4000	303.38778	312.10413
5000	379.23471	391.93729
6000	455.08164	472.52253
7000	530.92859	552.81858
8000	606.77562	632.96535
9000	682.62246	712.88647
10000	758.46941	792.60924
11000	834.31638	872.27845
12000	910.16327	952.16408
13000	986.01036	1016.89661
14000	1061.8572	1088.67746
15000	1137.70456	1157.67573
16000	1213.55113	1239.57779
17000	1289.39848	1310.41068
18000	1365.24491	1378.681
19000	1441.09241	1444.80897
20000	1516.93884	1530.8632
21000	1592.78619	1606.60486

A.2. Numerical values of plots of the steel beam

The numerical values of the forces and displacements in Figure 5.2 are shown in Table A.9. The buckling resistances are 8.27 kN and 827 kN. The other forces are factors of this buckling resistance. The used factors are 0.8, 0.9, 1.1, 1.12, 1.14, 1.16, 1.18 and 1.2.

Table A.9: Numerical values of Force-Displacement diagram in Figure 5.2.

F [kN] small-scaled	F [kN] real-sized	u_z [mm] small-scale	u_z [mm] real-sized
6.616	661.6	1.09829	10.98156
7.443	744.3	1.67933	16.78898
8.27	**827**	**2.82686**	**28.25405**
9.097	909.7	6.00543	59.98294
9.2624	926.24	7.4473	74.3619
9.4278	942.78	9.654	96.3515
9.5932	959.32	13.44789	134.11
9.7586	975.86	21.48799	213.9328
9.924	992.4	49.8826	493.71839

Tables A.10 and A.11 depict the linear and non-linear moments at midspan of the statically indeterminate beam.

Table A.10: Numerical data of the linear and non-linear moment at midspan of the small-scale statically indeterminate beam as shown in Figure 5.7.

Load[kN/m]	Linear moment midspan [kNm]	Non-linear moment midspan [kNm]
2	0.00167	0.00167
4	0.00333	0.00333
6	0.005	0.005
8	0.00666	0.00666
9.09	0.00757	0.00757
10	0.00833	0.01005
12	0.01	0.01485
12.1	0.01012	0.01522
14	0.01166	0.01984
16	0.01333	0.02484
18	0.015	0.02984
20	0.01666	0.03484

Table A.11: Numerical data of the linear and non-linear moment at midspan of the real-sized statically indeterminate beam as shown in Figure 5.7.

Load[kN/m]	Linear moment midspan [kNm]	Non-linear moment midspan [kNm]
20	1.66664	1.66664
40	3.33327	3.33327
60	4.9999	4.9999
80	6.66654	6.66654
90.9	7.57486	7.57486
100	8.33317	9.9013
120	9.99981	14.85442
121.2	10.0981	15.1566
140	11.66644	19.84865
160	13.33308	24.84899
180	14.99971	29.8496
200	16.66635	34.85576

Tables A.12 and A.13 depict the linear and non-linear nodal moments of the statically indeterminate beam.

Table A.12: Numerical values of the linear and non-linear nodal moments of the small-scale statically indeterminate beam as shown in Figure 5.8.

Load [kN/m]	Linear nodal moment [kNm]	Non-linear nodal moment [kNm]
2	-0.00334	-0.00333
4	-0.00666	-0.00666
6	-0.01	-0.01
8	-0.01332	-0.01333
9.09	-0.01515	-0.01515
10	-0.01666	-0.01495
12	-0.02	-0.01514
12.1	-0.02024	-0.01514
14	-0.02332	-0.01515
16	-0.02666	-0.01515
18	-0.03	-0.01515
20	-0.03332	-0.01515

Table A.13: Numerical values of the linear and non-linear nodal moments of the real-sized statically indeterminate beam as shown in Figure 5.8.

Load [kN/m]	Linear nodal moment [kNm]	Non-linear nodal moment [kNm]
20	-3.33327	-3.33327
40	-6.66654	-6.66654
60	-9.9998	-9.99981
80	-13.33308	-13.33308
90.9	-15.14971	-15.14971
100	-16.66634	-15.09822
120	-19.99962	-15.14501
121.2	-20.1962	-15.14282
140	-23.33288	-15.15068
160	-26.66616	-15.15024
180	-29.99942	-15.14954
200	-33.3327	-15.14328

Table A.14 depicts the maximum displacement of both the small-scale and the real-sized statically indeterminate beam.

Table A.14: Non-linear deformation of the small-scale and real-sized statically indeterminate beam as shown in Figure 5.10.

Small-scale structure		Real-sized structure	
Load [kN/m]	u_{max} [mm]	Load [kN/m]	u_{max} [mm]
2	0.12652	20	1.26577
4	0.25304	40	2.53154
6	0.37956	60	3.79731
8	0.50608	80	5.06307
9.09	0.57504	90.9	5.75292
10	0.88851	100	8.60353
12	1.4829	120	14.83569
12.15	1.52934	121.5	15.21322
14	2.10559	140	21.06488
16	2.72912	160	27.30317
18	3.35198	180	35.54186
20	3.97558	200	39.78884

A.3. Numerical values of plots of the steel Vierendeel girder

Tables A.15 and A.16 depict linear and non-linear horizontal displacements of node N8 of the steel Vierendeel girder.

Table A.15: Numerical values of linear and non-linear horizontal displacement of node N8 of the small-scale Vierendeel girder as shown in Figures 6.4 and 6.8.

Load [kN]	linear u_x of node N8 [mm]	non-linear u_x of node N8
1	0.19561	0.27739
2	0.39121	0.56933
3	0.58682	0.88061
4	0.78243	1.21808
5	0.97804	1.59291
6	1.17364	2.02412
7	1.36925	2.54667
8	1.56486	3.23232
9	1.76047	4.25539

Table A.16: Numerical values of linear and non-linear horizontal displacement of node N8 of the real-sized Vierendeel girder as shown in Figures 6.4 and 6.8.

Load [kN]	linear u_x of node N8 [mm]	non-linear u_x of node N8
100	1.95796	2.77468
200	3.91593	5.69682
300	5.87389	8.81134
400	7.83186	12.18762
500	9.78982	15.94362
600	11.74779	20.25349
700	13.70575	25.47651
800	15.66372	32.33211
900	17.62168	42.55822

Tables A.17 and A.18 depict the linear and non-linear moments at node N8 of both the small-scale and real-sized Vierendeel girder.

Table A.17: Numerical values of linear and non-linear moments at node N8 of the small-scale structure as shown in Figures 6.7 and 6.11.

Load [kN]	linear moment node N8 [kNm]	non-linear moment node N8 [kNm]
1	-0.04824	-0.04686
2	-0.09648	-0.09196
3	-0.14472	-0.13536
4	-0.19297	-0.17729
5	-0.24121	-0.21796
6	-0.28945	-0.25764
7	-0.33769	-0.29655
8	-0.38593	-0.33483
9	-0.43417	-0.37088

Table A.18: Numerical values of linear and non-linear moments at node N8 of the real-sized structure as shown in Figures 6.7 and 6.11.

Load [kN]	linear moment node N8 [kNm]	non-linear moment node N8 [kNm]
100	-48.24069	-46.88775
200	-96.48138	-91.95774
300	-144.72209	-135.35909
400	-192.9627	-177.2848
500	-241.20341	-217.7493
600	-289.44409	-257.4767
700	-337.68481	-296.54869
800	-385.9255	-334.82859
900	-434.16619	-370.88409

A.4. Numerical values of plots of the concrete two-way slab

Tables A.19 and A.20 depict the linear and non-linear stresses in the concrete two-way slab.

Table A.19: Numerical values of linear and non-linear 3D stresses of the small-scale two-way slab as shown in Figures 7.2 and 7.6.

Load [kN/m^2]	Linear 3D stresses [N/mm^2]	Non-linear 3D stresses [N/mm^2]
1	6	6
2	12	12
3	18	18
4	24	24
5	30.1	30
6	36.1	34.4
7	42.1	34.6
8	48.1	34.6
9	54.1	34.6
10	60.1	34.6
11	66.1	34.6
12	72.1	34.7
13	78.1	35.2
14	84.1	36.6

Table A.20: Numerical values of linear and non-linear 3D stresses of the real-sized two-way slab as shown in Figures 7.2 and 7.6.

Load [kN/m^2]	Linear 3D stresses [N/mm^2]	Non-linear 3D stresses [N/mm^2]
1	6	6
2	12	12
3	18	18
4	24	24
5	30.1	30
6	36.1	34.4
7	42.1	34.6
8	48.1	34.6
9	54.1	34.6
10	60.1	34.6
11	66.1	34.6
12	72.1	34.7
13	78.1	35.2
14	84.1	36.6

Tables A.21 and A.22 depict the linear and non-linear maximum deformation of the concrete one-way slab.

Table A.21: Numerical values of linear and non-linear maximum deformation of the small-scale two-way slab as shown in Figures 7.3 and 7.7.

Load [kN]	Linear u_{max} $[mm]$	Non-linear u_{max} $[mm]$
1	3.56213	3.56208
2	7.12427	7.12415
3	10.6864	10.68623
4	14.24853	14.24831
5	17.81067	17.81039
6	21.3728	21.38148
7	24.93493	25.28932
8	28.49707	30.18419
9	32.0592	38.13193
10	35.62133	54.50276
11	39.18347	106.7572
12	42.7456	349.19029
13	46.30773	1354.17295
14	49.86987	5041.27312

Table A.22: Numerical values of linear and non-linear maximum deformation of the real-sized two-way slab as shown in Figures 7.3 and 7.7.

Load [kN]	Linear u_{max} $[mm]$	Non-linear u_{max} $[mm]$
1	35.62133	35.62077
2	71.24266	71.24155
3	106.864	106.8623
4	142.4853	142.4831
5	178.1067	178.1039
6	213.728	213.8148
7	249.3493	252.8932
8	284.9707	301.8419
9	320.592	381.3193
10	356.2133	545.0276
11	391.8347	1067.572
12	427.456	3491.903
13	463.0773	13541.73
14	498.6987	50412.73

A.5. Numerical values of plots of the concrete shell roof

Tables A.23 and A.24 depict the linear and non-linear displacement of node N6 of the concrete shell roof. The shell roof has an imperfection following the buckling curve.

Table A.23: Numerical values of linear and non-linear displacements of node N6 of the small-scale shell roof following buckling data imperfections as shown in Figures 8.3 and 8.6.

Load [kN/m^2]	Linear u_{tot} node N6 [mm]	Non-linear u_{tot} node N6 [mm]
250	0.95318	1.02026
500	1.90637	2.20041
750	2.85955	3.59167
1000	3.81273	5.26989
1250	4.76592	7.35442
1500	5.7191	10.04661
1750	6.67228	13.72645
2000	7.62547	19.26502
2250	8.57865	-
2500	9.53183	-
2657.15	10.131	-
2750	10.48502	-

Table A.24: Numerical values of linear and non-linear displacements of node N6 of the real-sized shell roof following buckling data imperfections as shown in Figures 8.3 and 8.6.

Load [kN/m^2]	Linear u_{tot} node N6 [mm]	Non-linear u_{tot} node N6 [mm]
250	9.53183	10.20263
500	19.06367	22.00456
750	28.5955	35.91675
1000	38.12733	52.69925
1250	47.65916	73.54455
1500	57.19099	100.46611
1750	66.72283	137.26458
2000	76.25467	192.65025
2250	85.78649	-
2500	95.31833	-
2657.15	101.31003	-
2750	104.85016	-

Table A.25 depicts the non-linear deformation of node N6 of the concrete shell roof when the load has a global buckling imperfection. The buckling imperfections are 1 mm and 10 mm for the small-scale and real-sized shell roofs respectively.

Table A.25: Numerical values of non-linear displacement of node N6 of both the small-scale and real-sized concrete shell roofs as shown in Figure 8.10.

Load [kN]	Non-linear small-scale u_{tot} N6 [mm]	Non-linear real-sized u_{tot} N6 [mm]
250	1.02286	10.22858
500	2.20644	22.06486
750	3.60242	36.02429
1000	5.28754	52.87544
1250	7.38283	73.82834
1500	10.09404	100.94045
1750	13.81554	138.15549
2000	19.50216	195.02157

B

Explanation of Buckling Resistance Calculation in Eurocode 1993-1-1

The computation of the buckling resistance according to Eurocode 1993-1-1 is done with the following formulas (Welleman, n.d.). The relative slenderness is depicted in Equation B.1:

$$\bar{\lambda} = \frac{N_{pl}}{N_{Euler}} = \frac{f_y \cdot A}{\frac{\pi^2 EI}{l_{buc}^2}} \tag{B.1}$$

The relative slenderness is the relation between the plastic normal force resistance and Euler buckling. This relative slenderness is then used in an empiric Equation. The Φ-factor is computed in Equation B.2:

$$\Phi = \frac{1}{2}(1 + \alpha(\bar{\lambda} - 0.2) + \bar{\lambda}^2) \tag{B.2}$$

Where α is an imperfection factor depending on the material properties. The reduction factor χ follows in Equation B.3:

$$\chi = \frac{1}{\Phi + \sqrt{\Phi^2 - \bar{\lambda}^2}} \tag{B.3}$$

Finally, this reduction factor has to be multiplied by the cross-sectional area and the yield strength to obtain the buckling resistance according to Eurocode 1993-1-1. It is also divided by a safety factor γ_{M1}. However, this is equal to 1 and does not change the outcome. This is shown in Equation B.4:

$$N_{bRd} = \frac{\chi A f_y}{\gamma_{M1}} \tag{B.4}$$

The Python script used to compute the buckling resistance of the beam in Section 5.1 is shown in Listing B.1.

Listing B.1: Python script used to compute the buckling resistance of the steel beam according to Eurocode 1993-1-1.

```
import numpy as np

def relative_slenderness(fy, A, l_b, E, I):
    Npl = fy * A
    N_eul = (np.pi**2 * E * I) / l_b**2
    lab = np.sqrt(Npl / (N_eul))
    return lab

def phi(lab, alpha):
    return 0.5 * (1 + alpha * (lab  - 0.2) + lab**2)

def reduction_factor(phi, lab):
    return 1 / (phi + np.sqrt(phi**2 - lab**2))

def buckling_capacity(X, A, fy, gam1):
    return (X * A * fy) / (gam1 * 1000)

# general data
```

```
fy, E, gamma_1 = 355, 210000, 1

# Small-scaled structure

D_ss = 6.35 # mm
A_ss, l_b_ss = 0.25 * np.pi*D_ss**2, np.sqrt(200)

# moment of inertia
I_ss = 0.25 * np.pi * (0.5 * D_ss)**4

# The imperfection factor is c=0.49, this is the case for both cross-sections because both structures are modelled with S355 construction steel.
alpha = 0.49

# Relative slenderness
lab_ss = relative_slenderness(fy, A_ss, l_b_ss, E, I_ss)

# reduction factor
phi_ss = phi(lab_ss, alpha)
X_ss = reduction_factor(phi_ss, lab_ss)

# Buckling capacity
N_brd_ss = buckling_capacity(X_ss, A_ss, fy, gamma_1)

D_rs = 63.5 # mm
A_rs, l_b_rs = 0.25 * np.pi*D_rs**2, np.sqrt(2000)

# moment of inertia
I_rs = 0.25 * np.pi * (0.5 * D_rs)**4

# The imperfection factor is c=0.49, this is the case for both cross-sections because both structures are modelled with S355 construction steel.
alpha = 0.49

# Relative slenderness
lab_rs = relative_slenderness(fy, A_rs, l_b_rs, E, I_rs)

# reduction factor
phi_rs = phi(lab_rs, alpha)
X_rs = reduction_factor(phi_rs, lab_rs)

# Buckling capacity
N_brd_rs = buckling_capacity(X_rs, A_rs, fy, gamma_1)
```

C

Derivation of failure load of the statically indeterminate beam

A schematic representation of the beam is illustrated in Figure C.1.

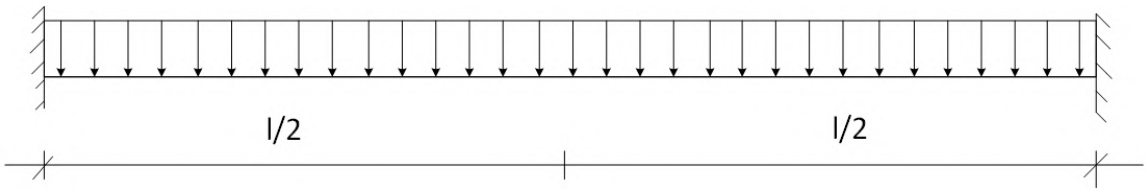

Figure C.1: Schematic model of the statically indeterminate beam.

The first failure load follows from the fact that the moment at the supports is $-\frac{1}{12}ql^2$ and the moment at midspan is $\frac{1}{24}ql^2$. The moments at the support will reach the plastic limit earlier because they are larger. By solving Equation C.1 we obtain the final failure load.

$$\begin{aligned} \frac{1}{12}ql^2 &= M_{pl} \\ q &= \frac{12M_{pl}}{l^2} \end{aligned} \tag{C.1}$$

The final failure load is computed with failure a failure mechanism. Hinges will be applied on the two supports and at midspan. Then a virtual displacement is applied. The schematic representation of the displaced structure is illustrated in Figure C.2.

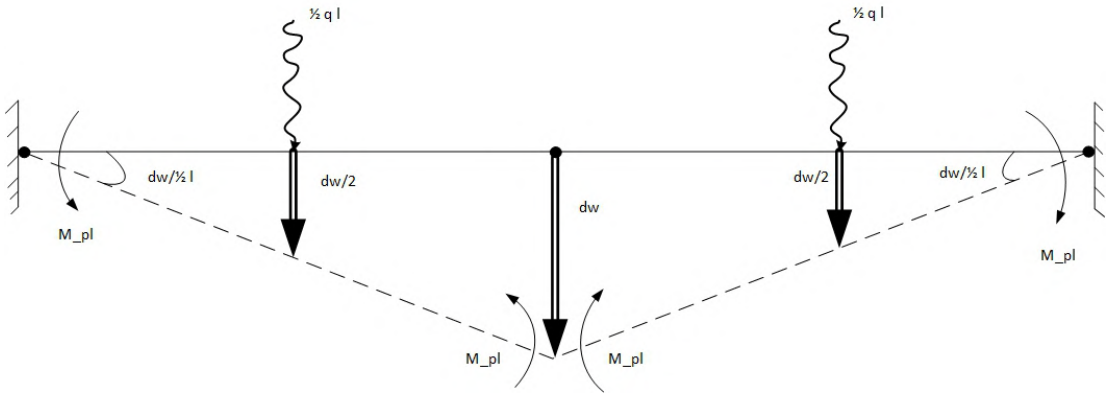

Figure C.2: Virtual work model for the statically indeterminate beam.

The principle of virtual work is shown in Equation C.2:

$$\partial A = 0 \tag{C.2}$$

The virtual work of this structure is derived in Equation C.3.

$$\partial A = -M_{pl} \cdot \frac{\partial w}{\frac{1}{2}l} + q \cdot \frac{1}{2}l \cdot \frac{\partial w}{2} - M_{pl} \cdot \frac{\partial w}{\frac{1}{2}l} - M_{pl} \cdot \frac{\partial w}{\frac{1}{2}l} q \cdot \frac{1}{2}l \cdot \frac{\partial w}{2} = 0 \tag{C.3}$$

By making q free we obtain the relation between the failure load and the plastic moment capacity. This is illustrated in Equation C.4:

$$q = \frac{4 \cdot M_{pl}}{\frac{1}{4}l^2} = \frac{16 M_{pl}}{l^2} \tag{C.4}$$